THERMAL ANALYSIS OF POWER LINES: METHODOLOGIES AND APPLICATIONS

Politecnico di Torino

Dottorato in Ingegneria Elettrica
Scienze elettriche

THERMAL ANALYSIS OF POWER LINES: METHODOLOGIES AND APPLICATIONS

Tesi di Dottorato

Supervisors:
Prof. Aldo CANOVA
Ing. Fabio FRESCHI

PhD candidate:
Ing. Alessandra GUERRISI
Student number: 169987

Ciclo XXV
Anno accademico 2012/2013

Contents

Introduction

The thermal analysis of cables aims at computing the temperature rise inside the cables due to the heat generated inside the conductor during the normal operation of the cable. The temperature limit of the cable is given by the insulation material: if this limit was exceeded the insulation would be damaged. For this reason it is necessary to calculate the cable ampacity that keeps the cable temperature under the insulation limit.
The heat generated by the conductor flows radially from inside to outside (the surrounding medium can be air or earth, in case of buried cable) through all the cable layers.
The cable ampacity is calculated solving a circuit that represents the thermal behaviour of the cable.
The Standards, in particular the Standard IEC 60287, consider many possible configurations. The Standard IEC 60287 allows to choose the cable (it is possible to specify the dimension and the material of each cable layer) and the layout (cables in air or buried). In case of underground cables, the user can decide how the cables are buried (directly in ground or in conduits), the material surrounding the system and the ambient temperature.
The Standard IEC 60287 has some lacks:

- it does not consider the presence of external heat sources in addition to the power line cables;
- it performs only a steady-state analysis;
- it is useful only when a tridimensional analysis is not necessary.

In the normal practice, in case of buried cables, it is not unusual that there are external heat sources in addition to the power line cables. And the power line is not always supplied by a costant current; it can be supplied by a load curve and there can be a transient. Moreover in some configurations the 2D section changes along the third dimension, therefore a 2D model is very conservative: a 3D analysis is useful.
In all these cases where the Standards are not applicable, another method can be applied. The numerical solver used allows to:

- consider any heat sources;

- study the transient behaviour;
- analize a 3D model.

The method has been applied to study a particular part of the power line: the junction zone. In the junction zone the magnetic field is higher and it can be necessary to shield the power line. The shielding method considered is the High Magnetic Coupling Passive Loop technology. If this system is applied a thermal analysis of the junction zone has to be performed because of the presence of a new set of conductors, in addition to the power line cables.
In this case the Standard IEC 60287 is not applicable because:

- there are heat sources different from the power line cables;
- a 3D model is necessary to study the effect of the ending connections of HMCPL and the cable joints.

Chapter 1

Standards for cable ampacity calculation

1.1 Neher-McGrath method

In 1957 Neher and McGrath published a paper that presented their method about the thermal analysis of cables [1]. The two authors have developped the work done by D. M. Simmons, that in 1932 had published a series of papers entitled "Calculation of the electrical problems of underground cables". In their paper Neher and McGrath considered also the developments happened in the cables sector in the following 25 years.
The Neher-McGrath (NM) method is a guide to calculate the temperature rise and the current-carrying capacity of cables. The NM method uses steady-state equations: the effect of operation under a repetitive cycle is considered, but the transient, due to a sudden application of a large load, is not considered.
The NM method is based on the application of the thermal equivalents of Ohm's and Kirchhoff's Laws to a simple circuit that represents the thermal behaviour of the cable (Fig. 1.1), therefore the thermal resistances of each cable layer and the heat source contributes must be calculated. Appendix I of [1] contains the equations to compute the

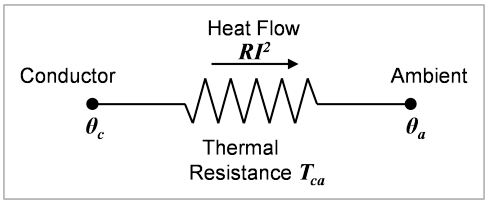

Figure 1.1: Thermal circuit of the cable.

thermal resistances for both single- and three-conductor cables for various installations (for example cable in air, cable in conduit in air, cable in duct, and cable direct earth

buried). In the case of buried cables it is also computed a resistance for the earth portion of the thermal circuit, that considers the mutual heating effect of the other cables of the system.
The heat produced by the conductor (RI^2) is not the only one loss contribute: in some cables additional heat contributes may be generated in the cable insulation and/or in the metallic shield raceway.
The temperature rise of the conductor above the ambient temperature is caused by the Joule losses (produced in the conductor, sheath and conduit) and by the dielectric losses:

$$\theta_c - \theta_a = \Delta\theta_c + \Delta\theta_d \tag{1.1}$$

where:

- θ_c is the conductor temperature;
- θ_a is the ambient temperature;
- $\Delta\theta_c$ is the temperature rise of the conductor due to the current produced losses;
- $\Delta\theta_d$ is the temperature rise of the conductor due to the dielectric losses.

Each of these temperature rises can be considered as the result of the heat flowing through a thermal resistance. The heat flow in the thermal circuit increases in steps because the losses occur at several points in the cable.
Therefore it is possible to express $\Delta\theta_c$ in this way:

$$\Delta\theta_c = W_c(T_i + q_s T_{se} + q_e T_e) \tag{1.2}$$

where:

- W_c is the losses portion developed in the conductor;
- T_i is the thermal resistance of the insulation;
- q_s is the ratio of the sum of losses in the conductor and sheath to the losses in the conductors;
- T_{se} is the total thermal resistance between sheath and conduit;
- q_e is the ratio of the sum of losses in the conductor, sheath and conduit to the losses in the conductors;
- T_e is the thermal resistance between the conduit and ambient.

At lower voltages the temperature rise due to dielectric losses is relatively small respect to the total temperature rise of the cable, but at higher voltages this contribute has to be considered. The resulting temperature rise due to the dielectric loss may be expressed as:

$$\Delta\theta_d = W_d \cdot T_{da} \tag{1.3}$$

where W_d is the losses portion developed in the dielectric and T_{da} is the effective thermal resistance between conductor and ambient for dielectric loss.
Eq. (1.2) can be written expressing the Joule losses in the conductor:

$$\Delta\theta_c = W_c \cdot T_{ca} = I^2 R_{DC}(1 + Y_c)T_{ca} \tag{1.4}$$

where:

- T_{ca} is the effective thermal resistance between conductor and ambient for conductor loss;
- R_{DC} is the DC resistance of the conductor;
- Y_c is a parameter that takes account of skin effect and proximity effect;
- $R_{DC}(1 + Y_c)$ represents the effective electrical resistance of the conductor.

From Eq. (1.1) and Eq. (1.4) the expression of the ampacity I follows:

$$I = \sqrt{\frac{\theta_c - (\theta_a + \Delta\theta_d)}{R_{DC}(1 + Y_c)T_{ca}}} \tag{1.5}$$

The ampacity of the cable is computed as function of the conductor temperature (depending on the insulation temperature limit) and considering the installation condition. In [2] the NM method is explained with some numerical examples. The ampacity is calculated in the case of aluminum and copper cables.

1.2 Standard IEEE 399-1997

The Chapter 13 “Cable ampacity studies” of the Standard IEEE 399-1997 [3] introduces a simplified method to calculate the cable ampacities, method already introduced in [4]. In the National Electric Code (NEC) [5] and in the Standard IEEE 835-1994 [6] the ampacity values are reported for some specific conditions:

- installation under an isolated condition;
- installation of groups of three or six circuits;

- soil thermal resistivity of 90 °C · cm/W;
- ambient temperature of 20 °C or 40 °C.

The Standard IEEE 399-1997 introduces the concept to apply a derating factor to a base ampacity to pass from the stated conditions to the installation conditions:

$$I' = F \cdot I \tag{1.6}$$

where:

- I' is the allowable ampacity under the actual installation conditions;
- F is the overall cable ampacity adjustment factor;
- I is the base ampacity, specified by the manafacturers or other authorative sources.

The overall cable ampacity adjustment factor F takes into account the differences in the cable's actual installation and operating conditions from the base conditions. It is composed of three components:

$$F = F_t \cdot F_{th} \cdot F_g \tag{1.7}$$

- F_t is the ambient and conductor temperature adjustment factor;
- F_{th} is the thermal resistivity adjustment factor;
- F_g is the grouping adjusment factor.

All these adjustment factors have been computed by a computer program based on the Neher-McGrath method. Then the adjustment factors tables were verified by utilizing the NEC, the Standard IEEE 835-1994 and the Underground Systems Reference Book [7].
In the Standard IEEE 399-1997 all the adjustment factors are reported.
The factor F_t is used to determine the cable ampacity when the operating ambient temperature and/or the maximum allowable conductor temperature differ from the original temperatures at which the cable base ampacity is specified. It is difficult to know the maximum operating ambient temperature: an estimate can be made considering historical meteorological data. For buried cable the ambient temperature is defined as the maximum soil temperature at the depth of installation at peak summertime. The soil temperature changes during the year, but these seasonal variations can be neglected when the cables are installed at a depth of 7–10 m.
The factor F_{th} is calculated based on the assumption that the soil has a uniform and constant thermal resistivity. The soil thermal resistivity varies in a wide range: from less than 40 °C · cm/W to more than 300 °C · cm/W. It depends on many factors (soil texture, moisture content, density, structural arrangements of the soil grains), but in

general higher density or moisture content of the soil results in a better heat dissipation and lower thermal resistivity.
The factor F_g takes into account the fact that grouped cables operate at a higher temperature than isolated cables, because there are more heat sources.
The ampacity value calculated with this manual method can be used as input for computer programs that implement more complex model. Many computer programs calculate cable temperatures for a given ampere loading, or a cable ampacities when the temperature is fixed.

1.3 Standard IEC 60287

The topic of the Standard IEC 60287 [8] is the calculation of the current rating in electric cables. It is applicable to the conditions of steady-state operation (100% load factor) of cables at all alternating voltages and direct voltages up to 5 kV.
The Standard is composed by eight parts:

- *Part 1-1* Current rating equations (100% load factor) and calculation of losses – General
- *Part 1-2* Current rating equations (100% load factor) and calculation of losses – Sheath eddy current loss factors for two circuits in flat formation
- *Part 1-3* Current rating equations (100% load factor) and calculation of losses – Current sharing between parallel single-core cables and calculation of circulating current losses
- *Part 2-1* Thermal resistance – Calculation of thermal resistance
- *Part 2-2* Thermal resistance – A method for calculating reduction factors for groups of cables in free air, protected from solar radiation
- *Part 3-1* Sections on operating conditions – Reference operating conditions and selection of cable type
- *Part 3-2* Sections on operating conditions – Economic optimization of power cable size
- *Part 3-3* Sections on operating conditions – Cables crossing external heat sources

In Part 1-1 the expression of the permissible current rating of cable is introduced, considering many possible cases:

- AC cables or DC cables;

- buried cables or cables in air;
- the occurring or not of the drying-out of the soil.

For all the possible cases the ampacity I is calculated. All the ampacity formulae come from the expression of the temperature rise above the ambient temperature (1.8), derived from the thermal circuit in Fig. 1.2:

$$\Delta\theta = (I^2R+1/2W_d)T_1+[I^2R(1+\lambda_1)+W_d]nT_2+[I^2R(1+\lambda_1+\lambda_2)+W_d]n(T_3+T_4) \quad (1.8)$$

where:

- $\Delta\theta$ is the conductor temperature rise above the ambient temperature (K);
- I is the current flowing in one conductor (A);
- R is the alternating current resistance, per unit lenght, of the conductor at maximum operating temperature (Ω/m);
- W_d is the dielectric loss, per unit lenght, for the insulation surrounding the conductor (W/m);
- T_1 is the thermal resistance, per unit lenght, between one conductor and the sheath ($\mathrm{K}\cdot\mathrm{m/W}$);
- T_2 is the thermal resistance, per unit lenght, of the bedding between sheath and armour ($\mathrm{K}\cdot\mathrm{m/W}$);
- T_3 is the thermal resistance, per unit lenght, of the external serving of the cable ($\mathrm{K}\cdot\mathrm{m/W}$);
- T_4 is the thermal resistance, per unit lenght, between the cable surface and the surrounding medium ($\mathrm{K}\cdot\mathrm{m/W}$);
- n is the number of load-carrying conductors in the cable (conductors of equal size and carrying the same load);
- λ_1 is the ratio of losses in the metal sheath to total losses in all the conductors in that cable;
- λ_2 is the ratio of losses in the armouring to total losses in all the conductors in that cable.

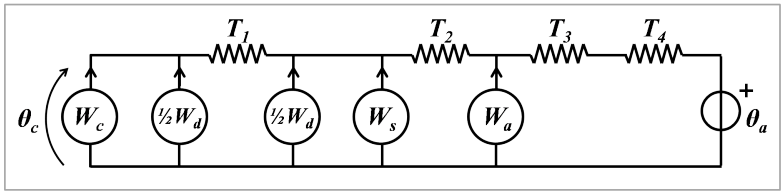

Figure 1.2: Cable thermal circuit (Std IEC 60287).

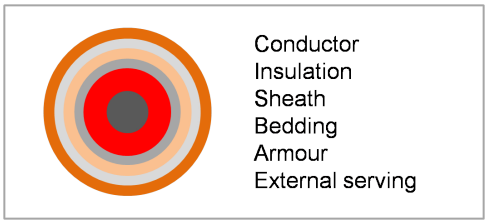

Figure 1.3: Cable layers considered in the Std IEC 60287.

In Fig. 1.3 all the possible layers of a cable, considered by the Standard IEC 60287, are represented, from the inner one (the conductor) to the outer one (the external serving). Eq. (1.9) computes the permissible current rating for AC cables, in the case of buried cables where drying out of the soil does not occur or in the case of cables in air. This expression derives from (1.8).

$$I = \left[\frac{\Delta\theta - W_d \left[0.5\ T_1 + n\ (T_2 + T_3 + T_4)\right]}{R\ T_1 + n\ R\ (1+\lambda_1) T_2 + n\ R\ (1+\lambda_1+\lambda_2)(T_3+T_4)} \right]^{0.5} \tag{1.9}$$

The second chapter of Part 1-1 of the Standard is about the losses produced by the cable during the operation. To consider the losses in the conductor (Joule losses) the AC resistance R is calculated, considering the skin effect and the proximity effect:

$$R = R'(1 + y_s + y_p) \tag{1.10}$$

where:

- R' is the DC resistance of the conductor at maximum operating temperature;
- y_s is the skin effect factor;
- y_p is the proximity effect factor.

Then the factors λ_1 and λ_2, introduced in (1.8), are calculated; they introduce, respectively, the loss in sheath and screen (caused by circulating currents and eddy currents) and the loss in the armour, reinforcement and steel pipes. To calculate λ_1 and λ_2 an iterative method is needed because the resistances R_S (AC resistance of the cable sheath)

and R_A (AC resistance of the armour) depend on the maximum operating temperatures θ_{sc} and θ_{ar}.
For the sheath:

$$R_S = R_{SO}[1 + \alpha_{20}(\theta_{sc} - 20)] \tag{1.11}$$

$$\theta_{sc} = \theta_c - (I^2R + 0.5\ W_d)\ T_1 \tag{1.12}$$

and for the armour:

$$R_A = R_{AO}[1 + \alpha_{20}(\theta_{ar} - 20)] \tag{1.13}$$

$$\theta_{ar} = \theta_c - \{(I^2R + 0.5\ W_d)\ T_1 + [I^2R(1 + \lambda_1) + W_d]\ n\ T_2\} \tag{1.14}$$

where:

- R_{SO} is the AC resistance of cable sheath or screen at 20 °C;
- R_{AO} is the AC resistance of armour at 20 °C;
- α_{20} is the temperature coefficient of electrical resistivity at 20 °C;
- θ_c is the maximum operating temperature of the conductor;
- W_d are the dielectric losses.

In Part 2-1 of the Standard the thermal resistances are calculated.
The Standard IEC 60287 has been used to analyze a test case. All the results are reported in Chapter 2.

Chapter 2

Numerical methods application

2.1 Steady-state analysis

The thermal analysis has been performed focusing the attention on the case of buried cables. The test case in made up of three buried cables in flat configuration. In Fig. 2.1 the layers of the cable and the layout analyzed are shown; in Tables 2.1 and 2.2 all the parameters of the test case are summarized. It has been considered moist compact ground as surrounding media, that has a thermal conductivity equal to 1 W/m/K, and an ambient temperature of 20 °C.
In this Paragraph the ampacity value for this specific configuration has been calculated considering three different methods: the Standard IEC 60287, a magneto-thermal analysis and DualLab. In Paragraph 2.2 the analysis has been completed studying the transient of the phenomenon.

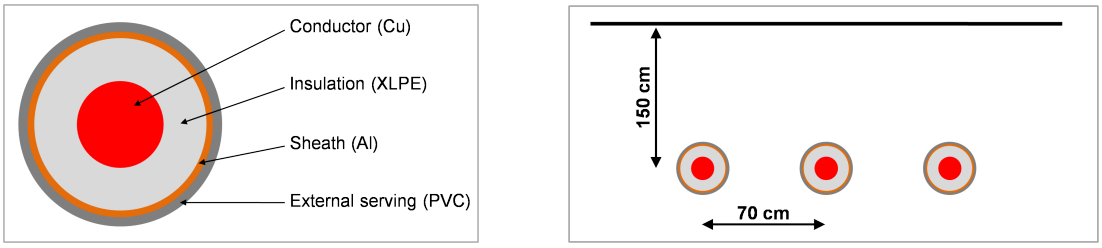

(a) (b)

Figure 2.1: Cable (a) and configuration (b) analyzed.

2.1.1 Standard IEC 60287

The Standard IEC 60287, introduced in the previous Chapter, has been implemented with a MATLAB code.

Table 2.1: Main parameters of the cable

Rated voltage	220 kV
Cross section	1600 mm^2
Insulation	XLPE

Table 2.2: Cable geometry

Layer	Diameter
Conductor	51.35 mm
Sheath	102.30 mm
Insulation	109.55 mm
External serving	121.00 mm

The Standard IEC 60287, in Part 1-1, intruduces the topic of the sheaths bonding to calculate che coefficient λ_1 that is the ratio of losses in the metal sheath to total losses. The Standard considers three possible methods to connect the sheaths (single-point bonding, cross bonding and both ends bonding) and computes the cable ampacity for seven different cases (Table 2.3) that differ from each other in the sheath bonding. The three sheath bonding methods are introduced in [9].
Bonding the sheaths in a proper way reduces the losses in the sheaths. The easiest method is the single point bonding: the sheaths are in open circuit (Fig. 2.2(a)). In this case one extremity is connected on earth and the other one is isolated; in this way there are not circulating currents because the sheaths circuit is open. The second method is the cross bonding: the sheath are transposed as shown in Fig. 2.2(c) and there are not circulating currents inside the circuit. On the other hand if the sheaths are bonded at both ends (solid bonding, Fig. 2.2(b)) the sheaths circuit is closed, so the induced currents can circulate inside the circuit producing losses for Joule effect.
The ampacity values obtained with the MATLAB code have been compared with the ampacity values calculated with a commercial software. This software implements the Standard IEC 60287 too and analyses the same cases considered in Table 2.3. The Standard IEC 60287 considers an isothermal earth surface, instead in the commercial code it is possible to choose between a isothermal and a non-isothermal earth surface, introducing the value of air ambient temperature.
The cable analyzed has an insulation in XLPE. The XLPE can be unfilled or filled: in case of filled XLPE the dielectric losses are 6 times bigger than the case of unfilled XLPE, therefore the ampacity values will be lower.
The results obtained with both the codes are comparable (Fig. 2.3 and 2.5). In case of single-point bonding (Case 1) and cross bonding (Cases 2–3) the ampacity values are

Table 2.3: Cases analyzed

Case 1	Sheats bonded at a single point
Case 2	Sheats cross-bonded, with regular transposition
Case 3	Sheats cross-bonded, without (regular) transposition
Case 4	Sheats bonded at both ends, with regular transposition, spacing even
Case 5	Sheats bonded at both ends, with regular transposition, spacing uneven
Case 6	Sheats bonded at both ends, without (regular) transposition, spacing even
Case 7	Sheats bonded at both ends, without (regular) transposition, spacing uneven

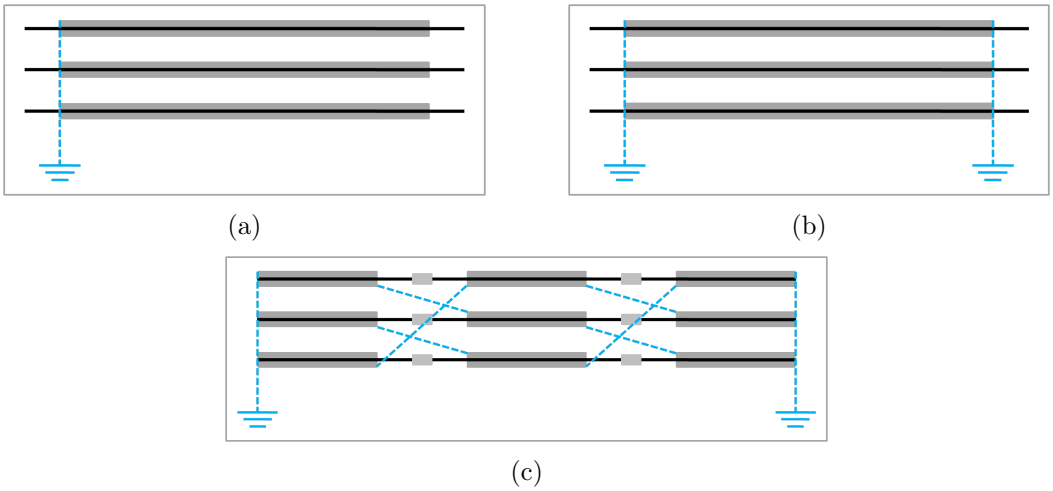

Figure 2.2: Sheaths bonding methods.

higher respect to the cases where the sheaths are bonded at both ends (Case 4–7) because these methods of sheath connection (single and cross bonding) reduce the circulating currents inside the sheaths. When the sheaths are bonded at both ends the overall losses inside the cable are higher and in particular the sheath losses are higher: these losses are not negligible because they exceed the losses in the conductor (Fig. 2.4 and 2.6).
It is interesting to evaluate the weight of each losses contribute, performing a thermal simulation that has the losses computed by the MATLAB code as input. In Table 2.4 the results are summarized. Two different temperature variations for each case has been considered (both for unfilled and filled XLPE cables): $\Delta\theta_{nil}$ that is the temperature variation neglecting the insulation losses and $\Delta\theta_{nsl}$ that is the temperature variation neglecting the sheath losses.
The simulations have been done introducing in the FEM model the same thermal parameters used in the Standard IEC 60287.
For unfilled XLPE cables the insulation losses are equal in all the seven cases (Fig. 2.4)

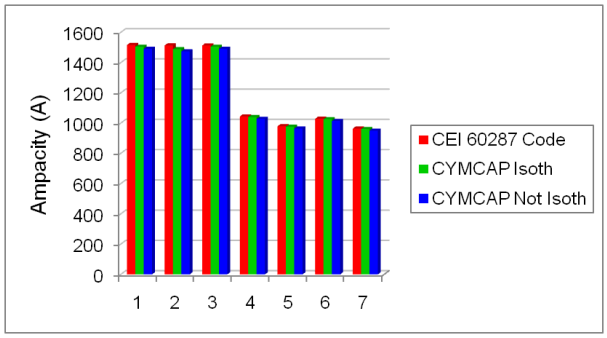

Figure 2.3: Ampacity values (unfilled XLPE).

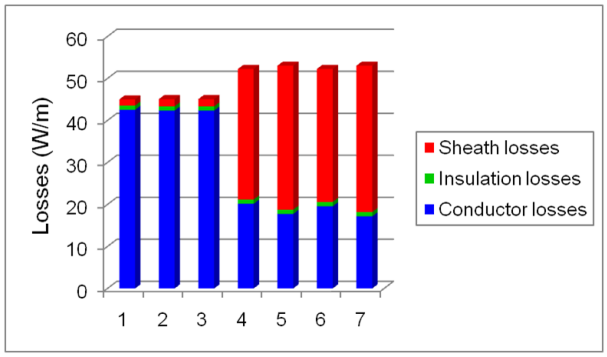

Figure 2.4: Losses values (unfilled XLPE).

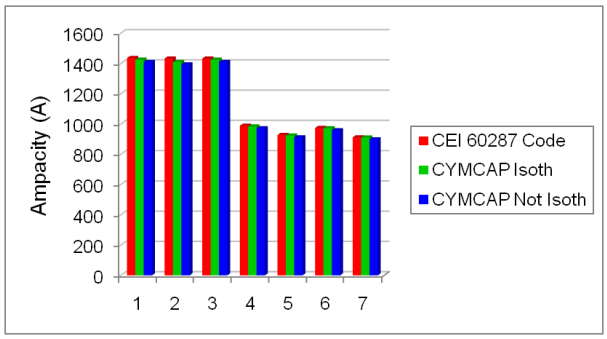

Figure 2.5: Ampacity values (filled XLPE).

and indeed, the fact of neglecting the insulation losses produces a temperature difference $\Delta\theta_{nil}$ that is equal in all the cases (1.3 °C). In case of single point bonding (Case 1) or cross bonding (Cases 2–3), the sheath losses and the insulation losses are comparable and the consequence is that the temperature differences obtained are comparable too (1.3 °C neglecting the insulation losses and 1.6 °C and 1.9 °C neglecting the sheath losses, respec-

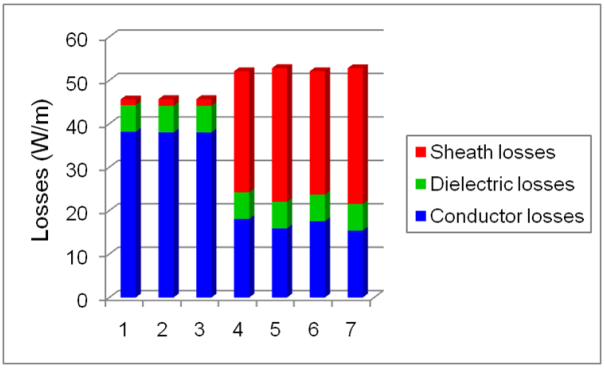

Figure 2.6: Losses values (filled XLPE).

tively, for single point and cross bonding); in case of cables bonded at both ends (Cases 4–7) the insulation losses do not change respect to the previous cases, but the sheath losses are higher and indeed the temperature difference neglecting these losses can reach 40 °C.
Also for filled XLPE cables the insulation losses are equal in all the seven cases (Fig. 2.6) and the temperature difference $\Delta\theta_{nil}$ does not change in all the cases (8 °C) and it is greater respect the case of unfilled XLPE (1.3 °C). The sheath losses are almost equal in the cases of single point and cross bonding and they produce a temperature differences comparable (respectively 1.5 °C and 1.7 °C). As in the case of unfilled XLPE, when the sheaths are bonded at both ends, the sheath losses increase and the temperature difference $\Delta\theta_{nsl}$ is greater ($32 - 36$ °C).
For unfilled XLPE cables, considering only the conductor losses produces a temperature reduction of 3 °C respect to the complete model (Cases 1–3); the temperature difference is higher for filled XLPE cables (9 °C) because the losses inside the dielectric are greater.
As example of each bonding sheaths method, Fig. 2.7 – Fig. 2.9 and Fig. 2.10 – Fig. 2.12 represent the temperature profile, respectively, for unfilled XLPE cables and filled XLPE cables, in case of single point bonding (Case 1), cross bonding (Case 2) and solid bonding (Case 4).

Table 2.4: Temperature variations

	Unfilled XLPE cable		Filled XLPE cable	
	$\Delta\theta_{nil}$ (°C)	$\Delta\theta_{nsl}$ (°C)	$\Delta\theta_{nil}$ (°C)	$\Delta\theta_{nsl}$ (°C)
Case 1	1.3	1.6	8	1.5
Case 2 – 3	1.3	1.9	8	1.7
Case 4 – 7	1.3	35 – 40	8	32 – 36

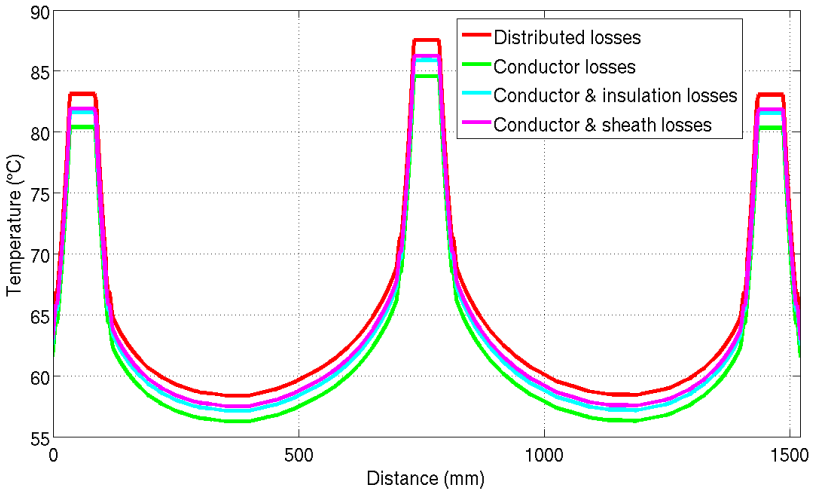

Figure 2.7: Case 1 - Sheaths bonded at a single point - Unfilled XLPE.

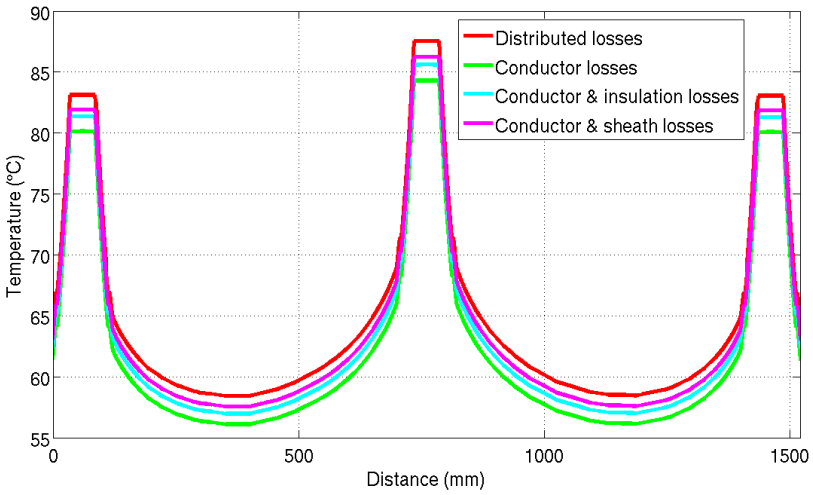

Figure 2.8: Case 2 - Sheaths cross-bonded - Unfilled XLPE.

2.1.2 Magneto-thermal analysis

The ampacity values obtained by the Standard IEC 60287 have also been compared with the ones calculated by a magnetic-thermal code. In Fig. 2.13 it is shown the schema of the iterative magnetic and thermal simulations performed by a FEM code. The simulations have been done introducing in the model the same parameters used in the Standard IEC 60287: electric parameters of conductor and sheath, thermal parameters of insulation and external serving; the missing data are from the Literature.

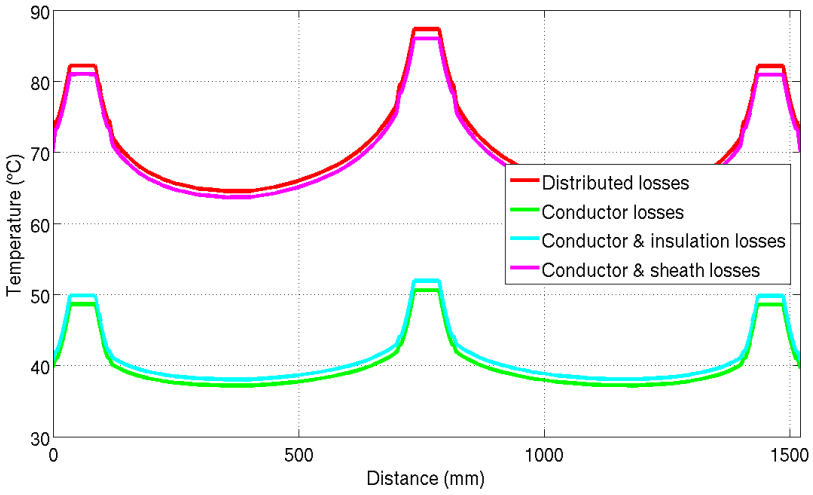

Figure 2.9: Case 4 - Sheaths bonded at both ends - Unfilled XLPE.

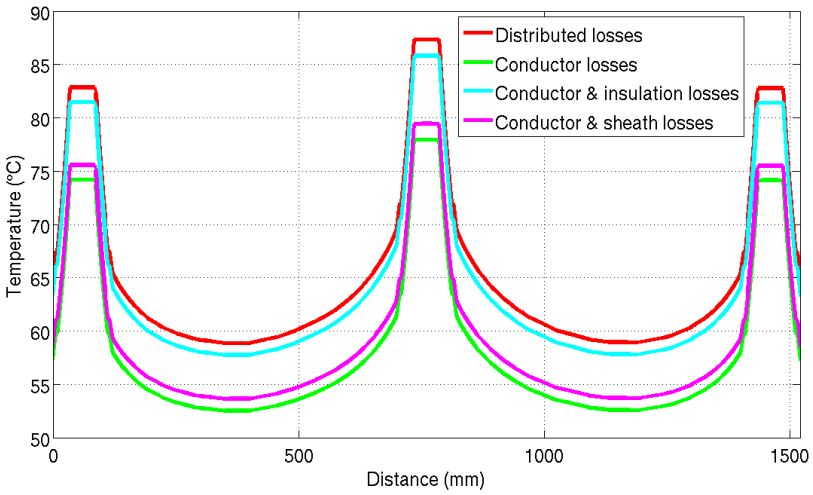

Figure 2.10: Case 1 - Sheaths bonded at a single point - Filled XLPE.

First of all a magnetic simulation has been performed and in the post-processing the Joule losses inside the conductors and the sheaths have been calculated. These losses are the heat sources of the thermal problem, that has been solved to obtain the temperature inside the conductors. The current I that brings one of the conductors to the thermal limit (90 °C) is the ampacity of the system I_z.
The Standard IEC 60287 considers the same value of sheath losses inside all the three cables; instead the sheath losses obtained by the FEM code are different: in the central

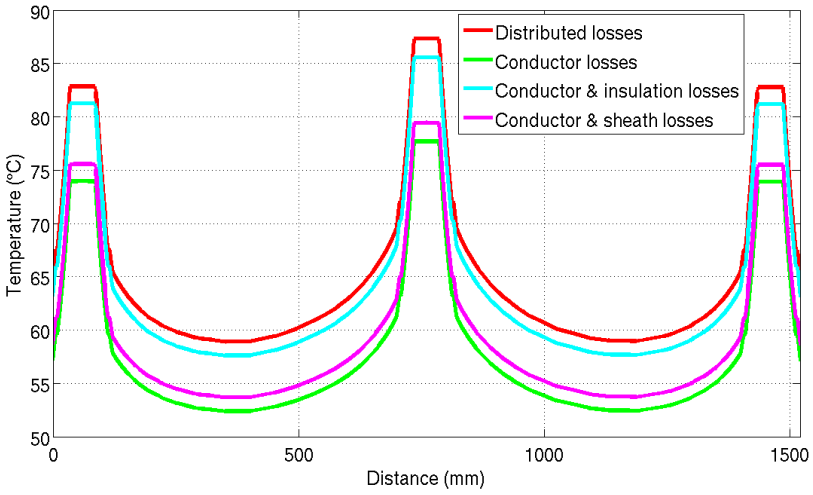

Figure 2.11: Case 2 - Sheaths cross-bonded - Filled XLPE.

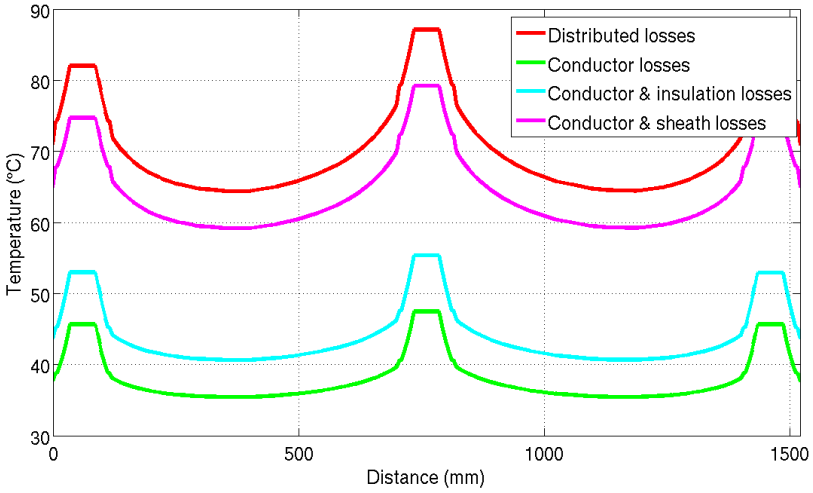

Figure 2.12: Case 4 - Sheaths bonded at both ends - Filled XLPE.

cable the sheath losses are 3.1% of the conductor losses, whereas in the external cables the sheath losses are 1.1% of the conductor losses (Tables 2.5 and 2.6). Considering the values obtained by the FEM code the sheath losses in the external cables are three times smaller than the sheath losses in the central cable.
The insulation losses, introduced in the model, has been calculated with the formula used in the Standard IEC 60287 (Part 1-1, Paragraph 2.2):

$$W_d = \omega \; C \; U_0^2 \; tan(\delta) \tag{2.1}$$

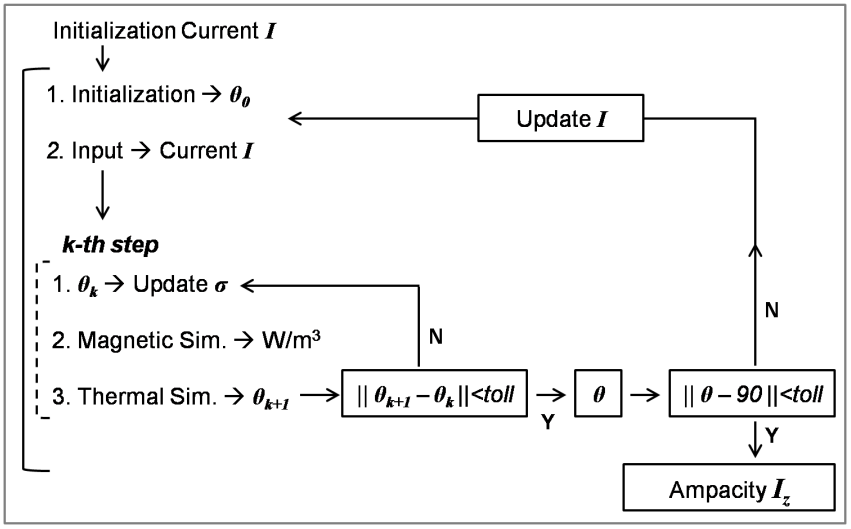

Figure 2.13: Iterations performed in the magnetic-thermal code.

Table 2.5: Conductor and sheath losses in unfilled XLPE cables

		Left cable	Central cable	Right cable
Conductor losses P_c	(W/m)	42.93	43.42	42.93
Sheath losses P_{sh}	(W/m)	0.47	1.36	0.46
Ratio P_{sh}/P_c	(%)	1.1	3.1	1.1

Table 2.6: Conductor and sheath losses in filled XLPE cables

		Left cable	Central cable	Right cable
Conductor losses P_c	(W/m)	38.77	39.21	38.77
Sheath losses P_{sh}	(W/m)	0.42	1.22	0.42
Ratio P_{sh}/P_c	(%)	1.1	3.1	1.1

where:

- $\omega = 2\pi f$;
- C is the capacitance per unit lenght (F/m);
- U_0 is the voltage on earth (V).

The value of parameter $tan(\delta)$ depends on the kind of insulation of the cable. In case of cables with insulation in XLPE this parameter is equal to 0.001 in case of unfilled XLPE

and 0.005 in case of filled XLPE.
Two different boundary conditions have been used: fixed temperature equal to 20 °C (boundary from ground to air) and null flux out of the boundary (at the end of the domain in the ground), as showed in Fig. 2.14.

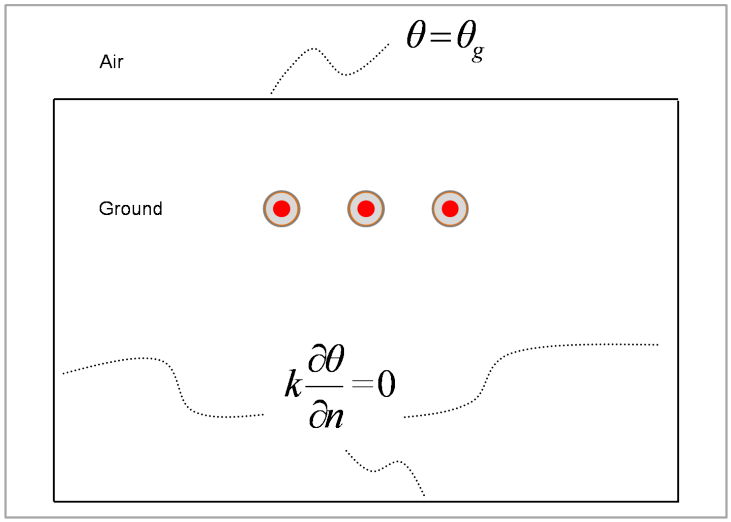

Figure 2.14: Boundary conditions.

The ampacity values calculated by the FEM code are higher than the ones obtained with the Standard IEC 60287:

- 1664 A for cables with insulation in unfilled XLPE;
- 1581 A for cables with insulation in filled XLPE.

2.1.3 DualLab

Finally the thermal simulations are performed by means of DualLab. DualLab is a collection of MATLAB routines that are useful to build numerical solvers for many physical theories. The toolbox is not an all-in-one program to solve a specific field problem, but rather an environment which makes the data structure available for implementing different formulations. Users must supply the initial discretization data (i.e. points coordinates, connectivity matrix and material codes), provided by standard mesh generators, and use the provided functions for building primal and dual data structures, incidence matrices and boundary conditions [10].
In the thermal analysis of power lines DualLab is a useful tool when it is not possible to apply the standards: for example when there are external heat sources in the model, in addition to the losses produced by the power line cables, or when it can be necessary a

tridimensional analysis of the model. These examples will be shown in Chapter 3.
For steady-state thermal problem the following equation has to be solved:

$$k\nabla^2\theta + q = 0 \tag{2.2}$$

where:

- k is the thermal conductivity (W/m/K);
- θ is the temperature (K);
- q is the volume heat generation (W/m^3).

The case analalyzed with DualLab is the same considered in the previous paragraphs: three cables buried in flat configuration. In particular, the same boundary conditions of the magnetic-thermal code have been used: fixed temperature and null flux (Fig. 2.14).
The heat sources considered in DualLab are the same used in the magneto-thermal code: Joule losses in the conductor and insulation, and dielectric losses in the sheath.
The temperature profiles obtained with the two codes are equal. In Fig. 2.15 the comparison between DualLab and FEM code is shown for unfilled XLPE cables.
This comparison is the first step for the next analysis: the study of the transient behaviour of the system.

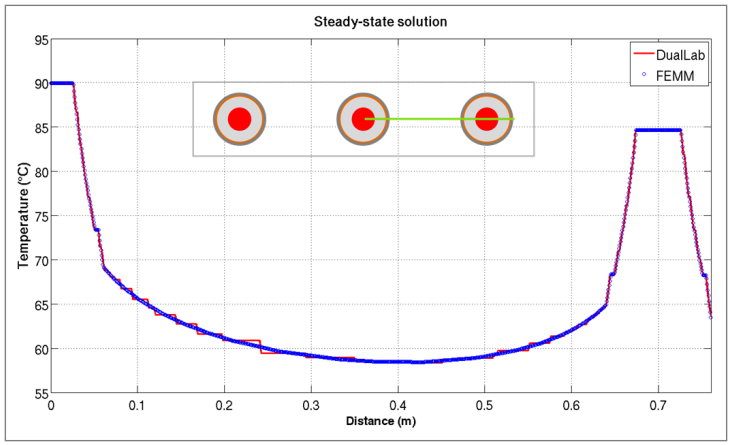

Figure 2.15: Comparison DualLab/FEM results (unfilled XLPE cable).

2.2 Transient analysis

After having performed a steady-state analysis, it can be interesting to study the evolution in the time of the phenomenon. This kind of analysis in not considered in the Standard

IEC 60287: the simulations have been performed with DualLab.
In order to take into account the thermal transient the time derivative of the temperature must be added to (2.2), obtaining:

$$-\rho c\frac{\partial\theta}{\partial t} + k\nabla^2\theta + q = 0 \tag{2.3}$$

where:

- ρ is the density (kg/m^3);
- c is the specific heat (J/kg/K);
- θ is the temperature (K);
- k is the thermal conductivity (W/m/K);
- q is the volume heat generation (W/m^3).

It has been considered the configuration with unfilled XLPE cables. The system analyzed has a time constant of 105 days. In Fig. 2.16 it is shown the trend of the transient to reach 98% of the steady-state temperature in the central point of the central cable, that thermally is the most stressed point.

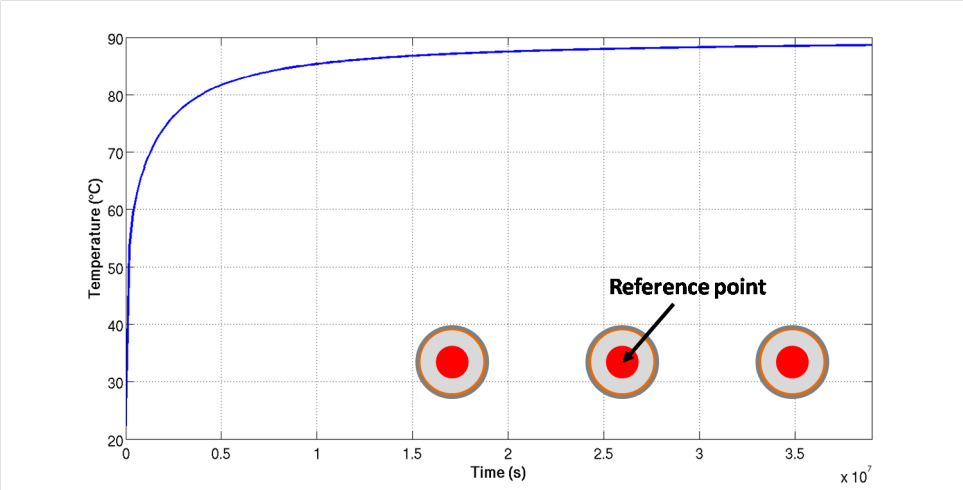

Figure 2.16: Transient in the reference point.

After having considered to supply the cables with a constant current, the system has been supplyed with a load profile. The load profile has been obtained from a real load curve, reshaping it to have a peak current value equal to the current value used in the previous simulations. The initial temperature of these simulations is the steady-state

temperature obtained by simulating the system supplied with a current equal to the r.m.s. value of the considered waveform. Supplying the power line with this load profile, the temperature profile is always under the temperature limit. In case of unfilled XLPE cables the maximum temperature reached is 67 °C, as shown in Fig. 2.17.

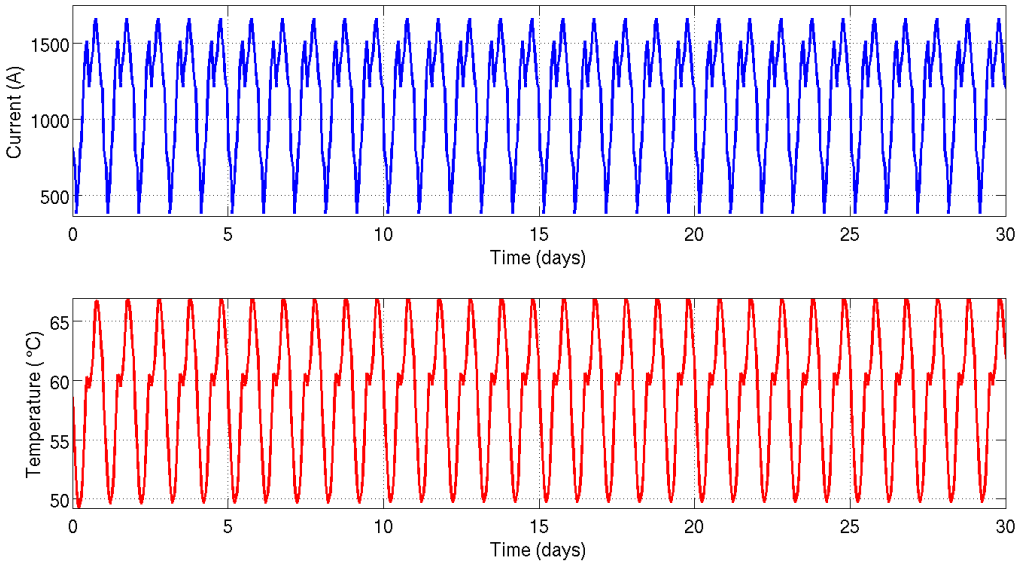

Figure 2.17: Reshaped load curve and temperature profile.

2.3 Discussion of results

The test configuration has been analyzed with three different methods.
The Standard IEC 60287 has been applied considering 14 different cases that differ from each other for the sheath bonding method (single point, cross and solid bonding) and for the insulation material (filled or unfilled XLPE). For each case the ampacity value has been calculated and the results obtained have been compared with the ones computed by a commercial code that also puts in practice this Standard.
Then the same configuration has been analyzed with a magneto-thermal code: after having solved the magnetic problem, the thermal simulation has been performed starting from the magnetic results (conductor and sheath losses). The ampacity values obtained are higher than the results obtained with the Standard: the Standard has a conservative approach.
The Standard IEC 60287 introduces only a steady-state analysis; a transient analysis has been performed by means of DualLab to calculate the time constant of the system and

to evaluate the behaviour of the system when it is supplied with a load profile.
It is important to remember the important effect, on the ampacity value, of the material where the cables are buried. The Standards usually suggest to consider the thermal resistivity of ground equal to 1 $m \cdot K/W$. Actually this parameter is very uncertain [11], [12] and it has a big influence on the ampacity value.
The same configuration analyzed in the previous paragraphs has been studied with the Standard IEC 60287 to evaluate the effect of the ground thermal resistivity on the ampacity value. It has been considered the configuration with sheaths cross bonded, with regular transposition (Case 2) and filled XLPE cables. In Table 2.7 the thermal resistivity values are reported for all the materials considered. In Fig. 2.18 the results obtained are summarized. Increasing the ground thermal resistivity from 0.5 $m \cdot K/W$ to 3 $m \cdot K/W$ the ampacity value halves. Therefore the kind of ground surrounding the cables has an high import and, at the same time, it introduces a parameter of uncertainty because it is not easy to know the soil characteristics (soil texture, moisture content, density, structural arrangemets) that influence the thermal resistivity value. Performing the simulations with magneto-thermal code the same trend is obtained (Fig. 2.18): increasing the thermal resistivity value the ampacity value decreases.

Table 2.7: Ground thermal resistivity

Material	Thermal resistivity ($m \cdot K/W$)
Moist sand Compact stone	0.5
Clayey ground Moist compact ground	1
Concrete	1.1
Bricks	1.2
Dry compact ground	2
Dry sand Gravel	3

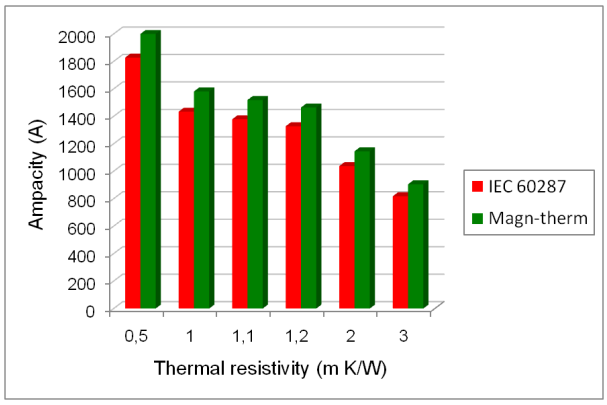

Figure 2.18: Ampacity vs ground thermal resistivity.

Chapter 3

Thermal analysis of HMCPL

3.1 Introduction

Electromagnetic pollution is an open subject because of the possible effects on human health and the electromagnetic compatibility issue. These are the reasons why magnetic field mitigation is an active field of research [13], [14]. A special type of conductive shield is represented by the passive loops. These shields are made of electrical conductors (typically the same electric cables used for transport and distribution) connected to each other in order to create closed loops. The working principle is based on electromagnetic induction: time varying magnetic fields, produced by AC currents, induce eddy currents in conductive loops and consequently they constitute an additional field source which modifies and attempts to reduce the main magnetic field produced by the sources. This kind of shield is used both for buried cable and overhead power lines [15]. In [16], [17], [18], [19], [20] a new concept of passive loop called the High Magnetic Coupling Passive Loop (HMCPL) was introduced along with a description of its magnetic performances.
HMCPL technology is very suitable for magnetic field mitigation of the junction. The cables are usually arranged in trefoil configuration but, when they need to be joined, the flat configuration has to be adopted because the joint needs larger spaces [20], a simple representation is shown in Fig. 3.1. It is worth noting that the use of the flat configuration leads to a higher magnetic field at ground level as shown in Fig. 3.2. This is the reason why the junction zone might need to be shielded.
To give a short overview of the HMCPL technique, the base layout is the one which associates a shielding conductor to each power cable as shown in Fig. 3.3. The magnetic cores allow the induction of currents inside the shielding circuit which are equal, to a first approximation, in amplitude but in phase opposition with respect to the source currents, so that the local magnetic field vanishes. When it is not possible to reach the power lines due to practical or technical problems (e.g. the need to shield an existing power line or shield a power line arranged in a trefoil configuration) the HMCPL could be

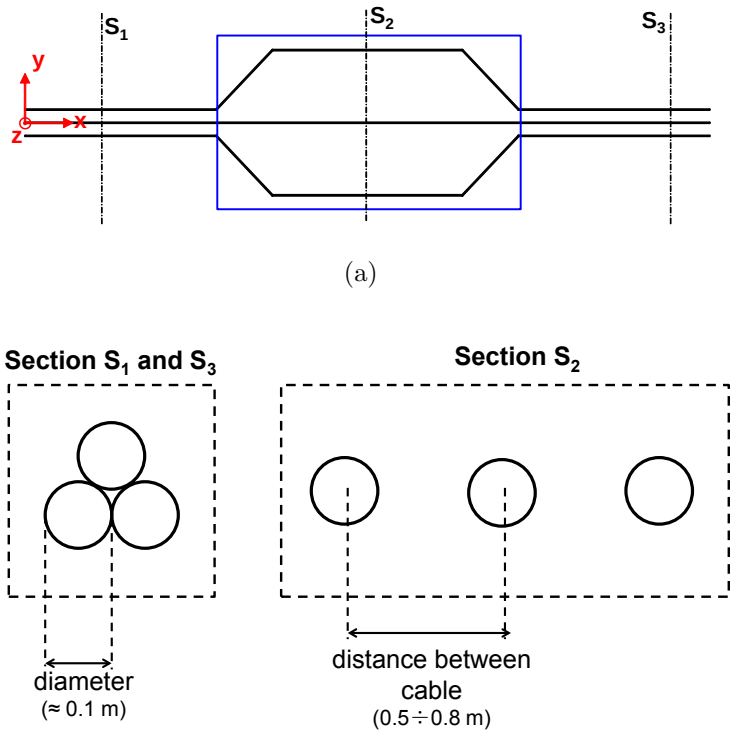

Figure 3.1: Classical layout of the junction zone (a) Cable sections (b).

used with a layout that employs a non-unitary coupling [16]. In this layout the shielding conductors are placed far from the source and they carry a current which is determined by a proper transformer ratio [16]. Therefore the design of this layout needs to be optimized to determine the position of the shielding conductors and the value of the transformer ratio [16]. The use of HMCPL technology imposes the introduction of a new set of conductors and, consequently, new Joule losses. Therefore a thermal analysis of the system is unavoidable in order to clarify whether the installation of a HMCPL leads to an ampacity derating of the power line or not [21].
The Standard IEC 60287 does not provide for the presence of external heat sources in addition to the power line, as in this case. The thermal behavior of a power line shielded with HMCPL has been studied with DualLab by means of steady-state and transient analysis and with some measurements.

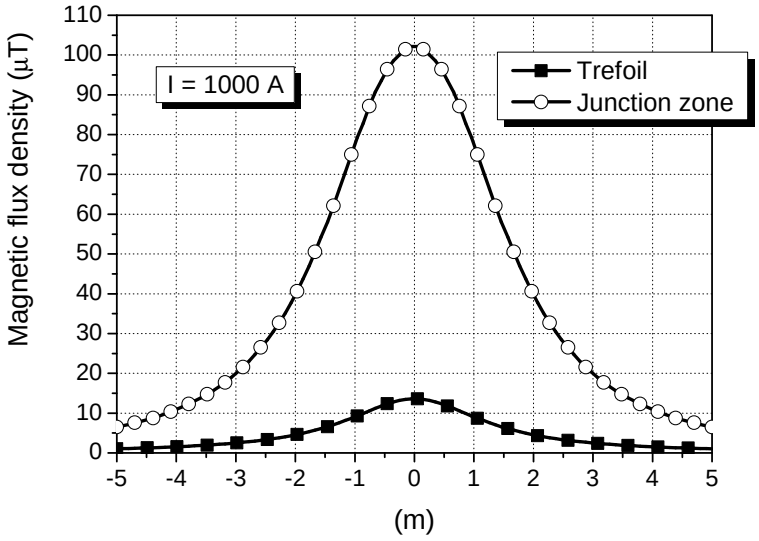

Figure 3.2: Magnetic induction at the ground level on a line orthogonal to the cables (Trefoil and Junction zone).

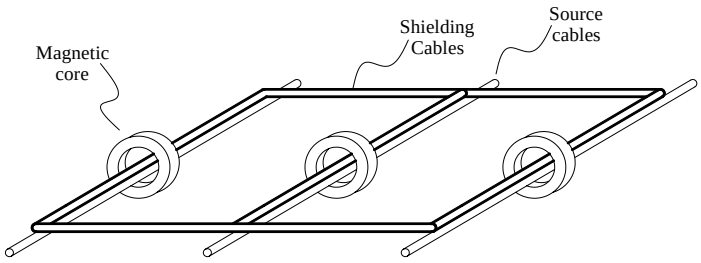

Figure 3.3: Geometrical layout of HMCPL with unitary coupling.

3.2 Thermal design of a power line

The thermal design of power system components is a challenging task. Several studies on power lines can be found in the Literature. The thermal equations are often analyzed by means of circuital approaches [22], [11], [23] or different numerical methods [24], [25], [26], [27], [28]. Many works consider the coupled magneto-thermal problem [22], [25], [29], [30]. In this Chapter, underground power cables are considered and the thermal problem is solved by means of numerical models thereby considering it as stand-alone uncoupled problem.
The power line to be designed is arranged for most of the path in trefoil configuration and, in correspondence of the junction zone, HMCPL technology is employed. Both cases are interesting because where the power line is arranged in a trefoil configuration the cables are strongly coupled from the thermal point of view. Within the junction zone the flat configuration is used and, consequently, the cables are less stressed from the thermal point of view. On the other hand flat configuration leads to a magnetic field at ground level which exceeds the suggested limits [31]. Therefore the HMCPL is used for lowering the magnetic field and a new verification of the thermal condition in the junction zone is needed.
In this section the power line in trefoil configuration is taken as a test case for the calibration of the model. The main parameters of the cable (represented in Fig. 3.4) are given by the manufacturer and they are summarized in Table 3.1. In this cable the airbag layer is employed. It is a new solution composed by extruded plastic layer that provides better mechanical protection than traditional metal armoured cable. It is designed and patented by the manufacturer and it is able to absorb the kinetic energy of a shock by plastic deformation. Finally, in Table 3.2 the thermal parameters of each layer are summarized.

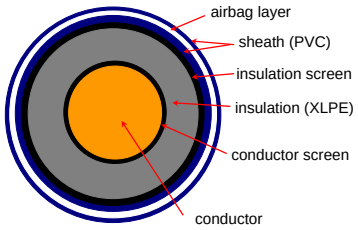

Figure 3.4: Main layers of the cable.

In trefoil configuration the cable ampacity is defined for installation 1.5 m below the ground level, considering cables in contact (distance between cables equal to their diameter) or cables in ducts (distance between cables equal to the diameter of the protective ducts, 200 mm).
The FEM model to be used is represented in Fig. 3.5 where the volume heat generation

Table 3.1: Main parameters of the cable

Rated Voltage	220 kV
Cross section	1600 mm^2
Insulation	XLPE

Table 3.2: Cable layers

Layer	Material	Thermal conductivity (W/m/K)
Conductor	Cu	386
	Al	237
Conductor screen	Al	237
Insulation	XLPE	0.29
Insulation screen	Al	237
Sheath	PVC	0.29
Airbag	Air	0.125
Sheath	PVC	0.29

(q) inside the cables could be computed by means of the AC resistance parameter given by the manufacturer.
Two different boundary conditions have been used: fixed temperature (boundary from ground to air) and null flux out of the boundary (at the end of the domain in the ground) [25], [24], [32].
The results are summarized in Table 3.3 and in Fig. 3.6 it is represented the temperature trend in case of copper cables, supplied with a current equal to 1480 A.

Table 3.3: Trefoil configuration ampacity

Conductor	Cables in contact	Spaced cables
Copper	1480 A	1531 A
Aluminium	1181 A	1222 A

In case of flat configuration the cables are placed at a distance of 700 mm (the same geometry that will be used with HMCPL); the ampacity values calculated are reported in Table 3.4. In Fig. 3.7 it is showed the temperature trend for copper cables in flat configuration supplied with a current equal to 1737 A.
The trefoil configuration is more limiting respect to the flat configuration from a thermal

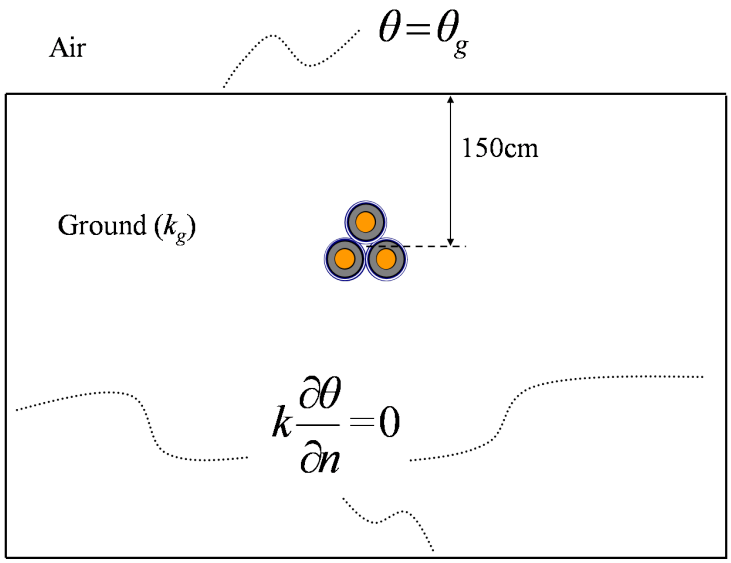

Figure 3.5: Trefoil configuration - FEM model.

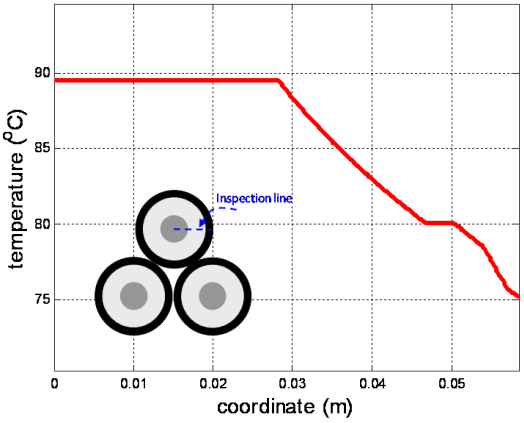

Figure 3.6: Temperature profile of the trefoil configuration (I_z = 1480 A).

Table 3.4: Flat configuration ampacity

Conductor	Ampacity value
Copper	1737 A
Aluminium	1384 A

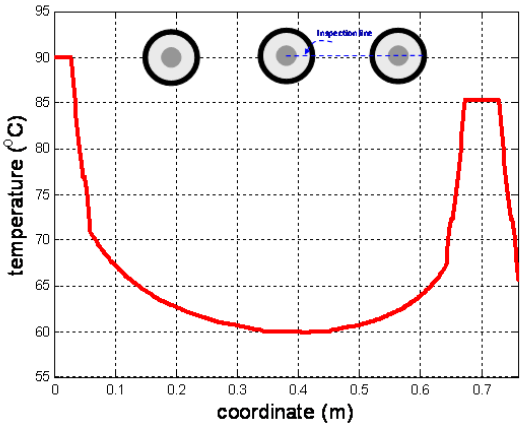

Figure 3.7: Temperature profile of the flat configuration (I_z = 1737 A).

point of view because the cables are closer. Supplying the cables in flat configuration whith the trefoil configuration ampacity (1480 A) the maximum temperature reached is equal to 72 °C (Fig. 3.8), that is far from the temperature limit. Therefore the thermal limit of the joint zone is the trefoil configuration ampacity.

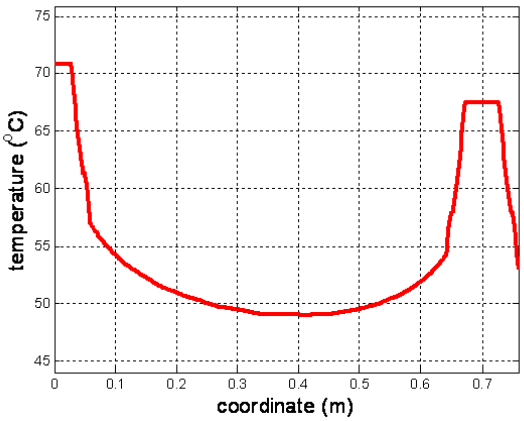

Figure 3.8: Temperature profile of the flat configuration (I_z = 1480 A).

3.2.1 Analysis sections HDD

In some cases the ampacity limit of the power lines is not set by the trefoil layout, but by some sections strongly stressed from a thermal point of view. This is the case of the sections where it is necessary to use the Horizontal Directional Drilling (HDD) to put

the cables in the ground. The cables can be buried at a maximum depth of 20 m and the distance between the cables varies from 0.5 m to 2 m. In Tables 3.5 and 3.6 all the ampacity values obtained by the simulation are summarized. In general both cables in copper and cables in aluminium buried at the depth over 10 m have an ampacity value lower than trefoil ampacity (1480 A for cables in copper and 1181 A for cables in aluminum) causing a derating of the power line. In Tables 3.5 and 3.6 the ampacity values lower than the trefoil ampacity value are highlighted.

Table 3.5: HDD sections - Ampacity values for Cu cables

Depth	Distance between cables			
	0.5 m	1 m	1.5 m	2 m
2 m	1611 A	1712 A	1794 A	1834 A
4 m	1489 A	1570 A	1611 A	1671 A
6 m	1407 A	1489 A	1530 A	1570 A
8 m	1367 A	1448 A	1489 A	1509 A
10 m	1347 A	1408 A	1448 A	1469 A
12 m	1326 A	1377 A	1408 A	1448 A
14 m	1306 A	1357 A	1387 A	1428 A
16 m	1286 A	1336 A	1367 A	1407 A
18 m	1266 A	1326 A	1347 A	1387 A
20 m	1255 A	1306 A	1347 A	1367 A

3.3 HMCPL steady-state simulation

The introduction of the HMCPL in the junction zone has been analyzed with reference to the model shown in Fig. 3.9. The parameter taken into account is the cross section of the shielding cables: 240 mm^2, 300 mm^2 or 400 mm^2. Phase splitting technique is used to improve the shielding efficiency [20] therefore the number of the shielding cables applied to a single source cable is also taken into account as a parameter (4 or 8, Fig. 3.9 represents 4 cables). In Table 3.7 the results obtained by varying cross section and number of shielding conductors are shown, for source cables with conductor in copper or aluminium. Most of the configurations lead to an ampacity lower than the trefoil ampacity (1480 A for copper cables and 1181 A for aluminium cables), this result means that the flat configuration with the HMCPL imposes a lower constraint on the ampacity with respect to the trefoil section, therefore the whole power line is subject to a derating.
The temperature profile in Fig. 3.10 shows that the central cable is the most stressed

Table 3.6: HDD sections - Ampacity values for Al cables

Depth	Distance between cables			
	0.5 m	1 m	1.5 m	2 m
2 m	1281 A	1375 A	1431 A	1469 A
4 m	1188 A	1244 A	1300 A	1319 A
6 m	1131 A	1187 A	1225 A	1262 A
8 m	1094 A	1150 A	1187 A	1206 A
10 m	1075 A	1122 A	1150 A	1178 A
12 m	1056 A	1094 A	1130 A	1150 A
14 m	1037 A	1075 A	1113 A	1131 A
16 m	1019 A	1066 A	1094 A	1112 A
18 m	1009 A	1056 A	1075 A	1103 A
20 m	1000 A	1037 A	1075 A	1093 A

Table 3.7: HMCPL ampacity values

HMCPL	Cu cables	Al cables
4 x 240 mm^2	1288 A	1125 A
4 x 300 mm^2	1360 A	1163 A
4 x 400 mm^2	1425 A	1213 A
8 x 240 mm^2	1473 A	1238 A
8 x 300 mm^2	1505 A	1263 A
8 x 400 mm^2	1565 A	1286 A

thermally.
To obtain a reduction of the temperature of the central cable it is possible to adopt different layouts that have a greater overall section of the shielding cables around the central cable: this can be done increasing the number of shielding cables or their section. For each HMCPL configuration all the possible solutions have been identified and analyzed. In Tables 3.8 and 3.9 the new ampacity values are summarized. Introducing more cables and/or cables with a greater section the ampacity values obtained are higher respect to the ampacity values of the base case with the same HMCPL solution for all the three cables of the power line (the values are reported in the first column of Tables 3.8 and 3.9).
In Fig. 3.11 it is shown the temperature profile when the external cables are shielded with

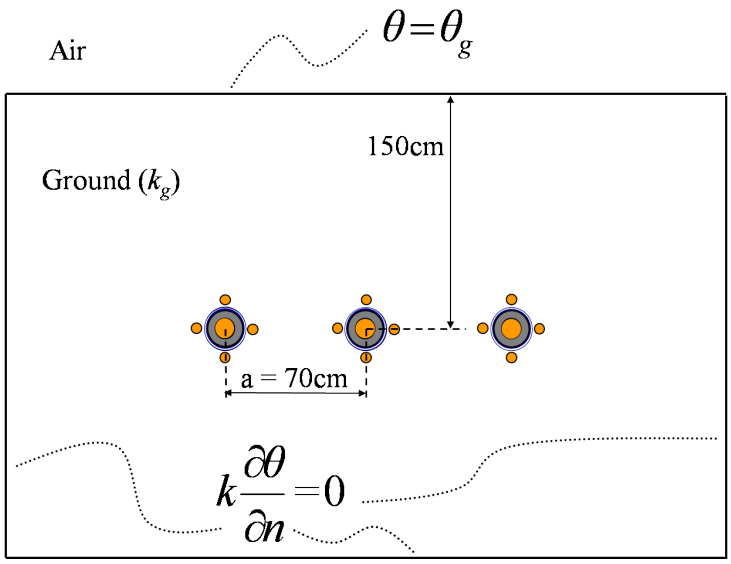

Figure 3.9: HMCPL - FEM model.

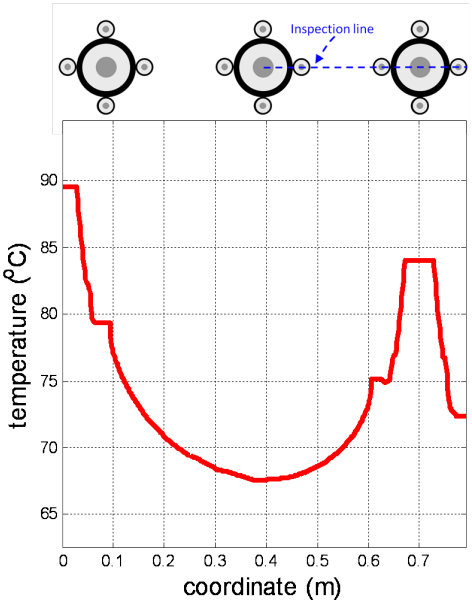

Figure 3.10: Steady-state solution along the reference line (4 x 240 mm^2 - I_z = 1288 A).

Table 3.8: HMCPL ampacity values for copper cables

HMCPL configuration	Variations of the central cable				
	4 x 300 mm^2	4 x 400 mm^2	8 x 240 mm^2	8 x 300 mm^2	8 x 400 mm^2
4 x 240 mm^2 (1288 A)	1326 A	1360 A	1380 A	1393 A	1401 A
4 x 300 mm^2 (1360 A)	n.a.	1392 A	1413 A	1433 A	1454 A
4 x 400 mm^2 (1425 A)	n.a.	n.a.	1437 A	1469 A	1493 A

Table 3.9: HMCPL ampacity values for aluminium cables

HMCPL configuration	Variations of the central cable				
	4 x 300 mm^2	4 x 400 mm^2	8 x 240 mm^2	8 x 300 mm^2	8 x 400 mm^2
4 x 240 mm^2 (1125 A)	1148 A	1170 A	1183 A	1194 A	1207 A
4 x 300 mm^2 (1163 A)	n.a.	1191 A	1203 A	1215 A	1230 A
4 x 400 mm^2 (1213 A)	n.a.	n.a.	1225 A	1237 A	1253 A

HMCPL in configuration 4 x 240 mm^2 and the central cable is shielded with HMCPL in configuration 4 x 400 mm^2.

3.4 HMCPL transient analysis

Even if the steady-state analysis seems to impose a derating for most of the configurations, a transient analysis is necessary in order to clarify if this derating needs to be imposed on the system or not.
The configurations already studied in steady-state conditions have again been analyzed in order to:

- calculate the thermal time constant of the system;
- calculate the "time limit" (i.e. the time needed to reach the temperature of 90 °C).

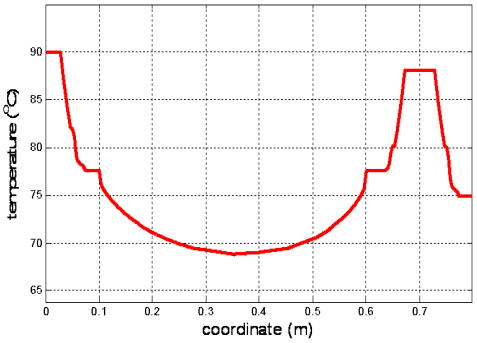

Figure 3.11: Steady-state solution (4 x 240 mm^2 for the external cables, 4 x 400 mm^2 for the central cable - I_z = 1360 A).

Finally, for the most critical system (configuration 4 x 240 mm^2) some simulations have been done taking into account the load profile of the power line.

3.4.1 Time constant calculation

In each configuration the system is supplied by a current equal to the ampacity I_z. The ampacity values have been computed in the steady-state simulations (Table 3.7).
In Table 3.10 the results of this transient analysis are shown. As is expected, the steady-state temperature is equal to 90 °C for all the configurations but, a very important result is that, the exponential behavior which leads to the steady-state temperature presents a time constant that varies from 120 days to 130 days.
In all the simulations the average values of specific heat and density of ground are considered: c = 1050 J/kg/K and ρ = 2000 kg/m^3. When the simulations are performed with the minimum values of specific heat and density of ground (c = 700 J/kg/K and ρ = 1400 kg/m^3) [11] the time constant is halved to 62 days (in the case of copper cables with HMCPL in configuration 4 x 240 mm^2) which is much larger than the load profile periodicity. The high value of the thermal constant time is confirmed by the bibliographic data where simulations [33] and measurements [23] lead to a transient of several days.

3.4.2 Time limit calculation

It is interesting to analyze how much time is needed to reach the limit temperature of 90 °C if the system is supplied with a higher current than its ampacity. This analysis is aimed at understanding if the derating evaluated with the steady-state analysis is really necessary or not. Therefore, each system is supplied with a current equal to the ampacity of the trefoil configuration (1480 A for copper cables and 1181 A for aluminium cables) and the following results are presented:

Table 3.10: Time constant

HMCPL	Cu cables	Al cables
4 x 240 mm^2	133 days	128 days
4 x 300 mm^2	130 days	125 days
4 x 400 mm^2	127 days	122 days
8 x 240 mm^2	125 days	121 days
8 x 300 mm^2	122 days	119 days
8 x 400 mm^2	120 days	117 days

- steady-state temperature θ_{steady} of the most thermally stressed conductor (the central one);
- time limit: the time needed to reach 90 °C.

The results for each configuration are summarized in Table 3.11 and in Fig. 3.12 the steady-state solution is shown in case of copper cables with HMCPL in configuration 4 x 240 mm^2 supplied with a current equal to 1480 A. In all the simulations the initial temperature is set to $\theta_0 = 20$ °C and the source current is equal to the trefoil ampacity value. The time needed to reach the limit of 90 °C and the final temperature θ_{steady} depends on the number and the section of shield conductors.

Table 3.11: Time limit and steady-state temperature

HMCPL	Cu cables		Al cables	
configuration	t_{90} (days)	θ_{steady} (°C)	t_{90} (days)	θ_{steady} (°C)
4 x 240 mm^2	7	111.9	24	97
4 x 300 mm^2	12	103.6	71	91.8
4 x 400 mm^2	31	95.5	n.a.	n.a.
8 x 240 mm^2	140	91.3	n.a.	n.a.
8 x 300 mm^2	n.a.	n.a.	n.a.	n.a.
8 x 400 mm^2	n.a.	n.a.	n.a.	n.a.

As shown in Table 3.11 this kind of simulation is not significant in some cases because the ampacity values calculated (Table 3.7) are greater than the trefoil ampacity values (Table 3.3), therefore it is known that the steady-state temperature is 90 °C and that this temperature will be got at the end of the transient.

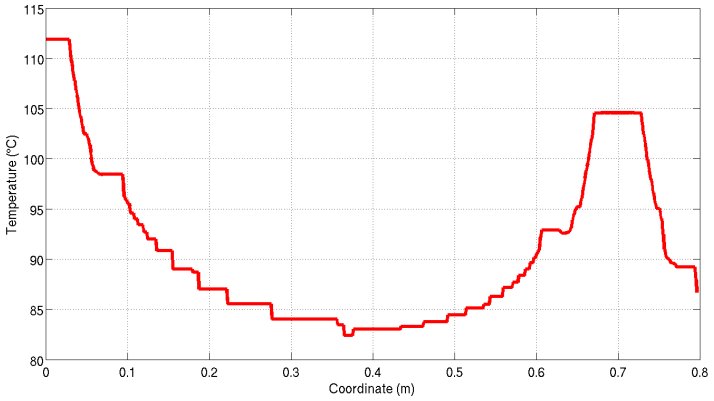

Figure 3.12: Steady-state solution along the reference line (4 x 240 mm^2 - I_z = 1480 A).

3.4.3 Simulations with power line load profiles

In the previous simulations the system was supplied by a constant current while in the following simulations the system is supplied by a load curve. The configuration 4×240 mm^2 has been considered. The actual load profile of a power line was measured over one day and, for the simulations, it was scaled in order to keep the shape but changing the peak value.
The initial temperature θ_0 of these simulations is the temperature θ_{steady} obtained by simulating the system supplied with a current equal to to the r.m.s. value of the considered waveform.
Both for copper and aluminium cables it has been considered two different cases: peak value equal to the ampacity value of the system with HMCPL (1288 A for copper cables and 1125 A for aluminium cables) and peak value equal to the trefoil ampacity value (1480 A for copper cables and 1181 A for aluminium cables).
In the first case (peak value equal to the ampacity value of the system with HMCPL) the temperature limit is not reached both for copper cables and aluminium cables (Fig. 3.13 and 3.15). Also in the second case (peak value equal to the trefoil ampacity value) the temperature limit is not reached for both the kinds of cables (Fig. 3.14 and 3.16). Therefore in all the cases the temperature reached supplying the power line with a load profile is very far from the temperature reached supplying the power line with the corresponding constant current. This means that cases considered unfeasible, because they brought to a derating of the power line, can be considered feasible with this analysis.

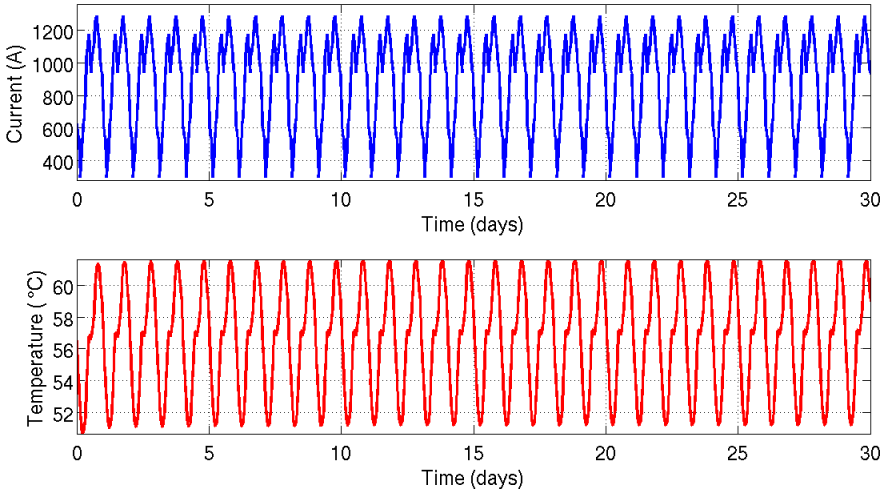

Figure 3.13: Reshaped load curve (Cu - 4 x 240 mm^2 - I_z = 1288 A).

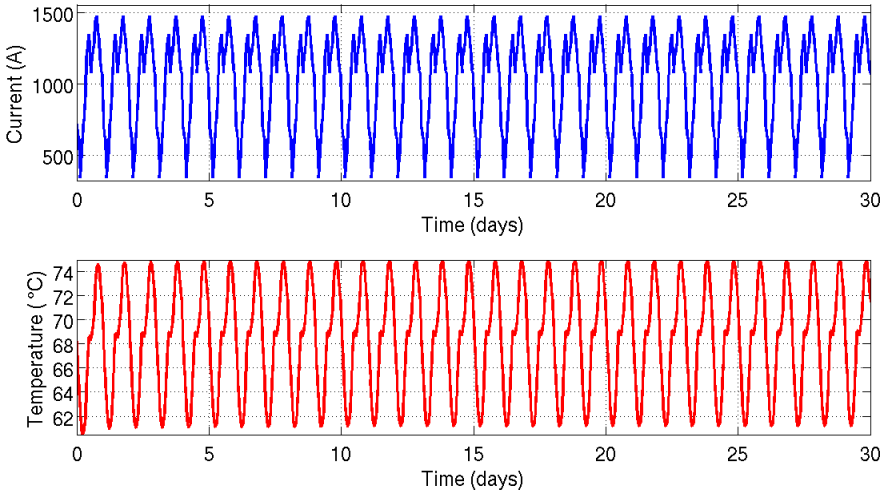

Figure 3.14: Reshaped load curve (Cu - 4 x 240 mm^2 - I_z = 1480 A).

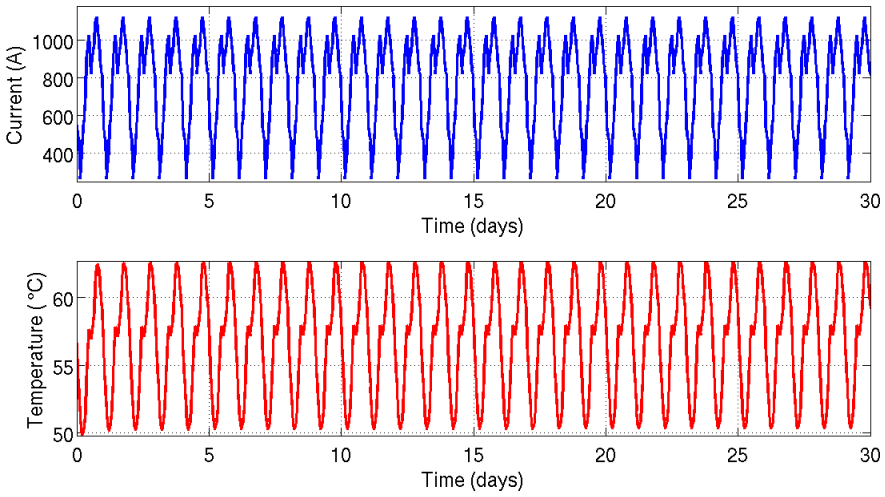

Figure 3.15: Reshaped load curve (Al - 4 x 240 mm^2 - I_z = 1125 A).

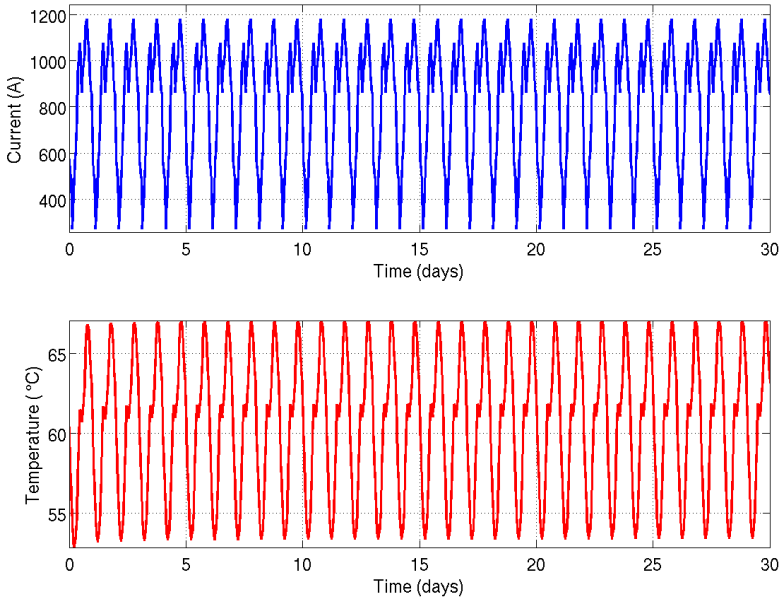

Figure 3.16: Reshaped load curve (Al - 4 x 240 mm^2 - I_z = 1181 A).

3.5 Tridimensional analysis

3.5.1 Effect of the ending connections

The ending connections of the HMCPL system must be taken into account during the design of the shield. To maximize the magnetic performances the ending connections should be placed as close as possible to the trefoil conjunction but, on the other hand the higher vicinity of the group of cables can create a thermal "hot spot". In order to investigate the influence of the ending connections on the global thermal behavior a 2D model is not sufficient: it is a good approximation (at least conservative) in order to design the HMCPL in the center of the junction zone but it is not representative for the analysis of the edge effect (i.e. when the shielding conductors reach the ending connection). Therefore a 3D model has been created and the analysis is performed for a steady-state configuration designed in order to keep the temperature below the defined limit (90 °C) in all the system.
The 3D model has been validated making a comparison with the results obtained with the 2D model. For the 3D simulations a simplified cable has been considered. It is constituted only by the conductor and the insulation because the presence of thin layers (as the insulation screen and the conductor screen) would produce a very high number of elements introducing numerical instabilities in the model. The conductor of the simplified cable has the same dimension of the conductor of the complete cable. All the other layers of the complete cable have been considered, in the simplified cable, as only one insulation layer (Fig. 3.17). The configuration analyzed is realized with source cables with conductor in copper and HMCPL in configuration 4 x 240 mm^2. The validation has

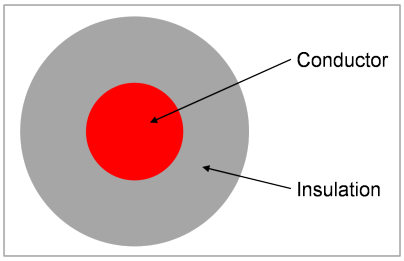

Figure 3.17: Simplified cable for 3D analysis.

been done analyzing both the 2D model and the 3D model and comparing the results obtained; in Fig. 3.18 it is shown, in red, the inspection line where the temperature has been calculated to compare the results obtained with the two models. The temperature profiles of both models are shown in Fig. 3.19: the results coincide, therefore the 3D model can be applied for more complex simulations.
For the analysis of the ending connections, due to symmetry reason, the whole domain can be reduced to 1/4 of the domain by using the proper boundary conditions. It has

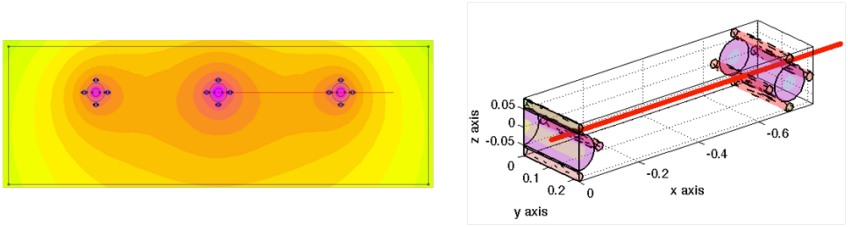

Figure 3.18: 2D model (right), 3D model (left).

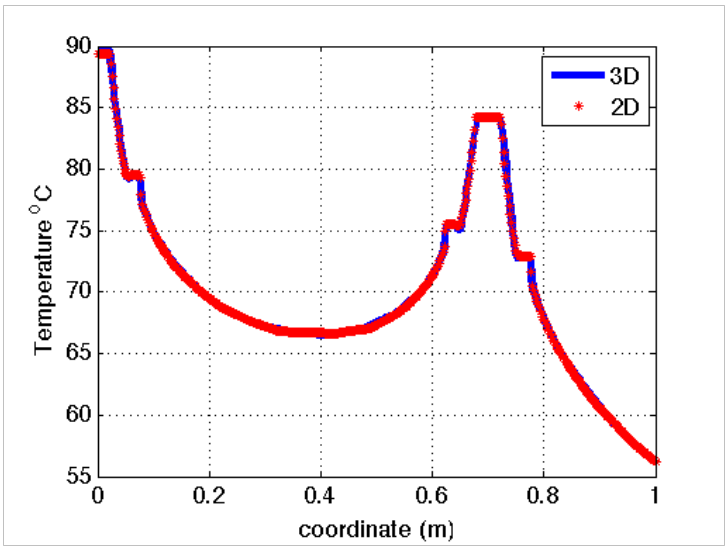

Figure 3.19: Results comparison between 2D and 3D model.

to be stressed that the final realization of the HMCPL takes into account 4 ending connections because it can be realized by two subsystems: six lower cables and six upper cables connected at both ends with a short circuit as represented in Fig. 3.20(a) [34]. The decoupling of the HMCPL in two subsystems does not affect the magnetic behavior and, moreover, it allows to employ a final ending connection realized as shown in Fig. 3.20(b). It is made by a flexible cable with three conductive plates where it is possible to fix six cable lugs. Moreover it is possible to use an epoxy resin which assures the protection against corrosion.
The analyzed domain is represented in Fig. 3.21. The meshed domain and an example of the total thermal field are represented in Fig. 3.22.
By means of a 3D model it is possible to plot the temperature profile along three interesting lines: the first one is centered with respect to the junction zone, the second one is placed prior to the conjunction of the power cables and the third one is located exactly between two ending connections. The three lines are represented in Fig. 3.23 and the results are summarized in Fig. 3.24.

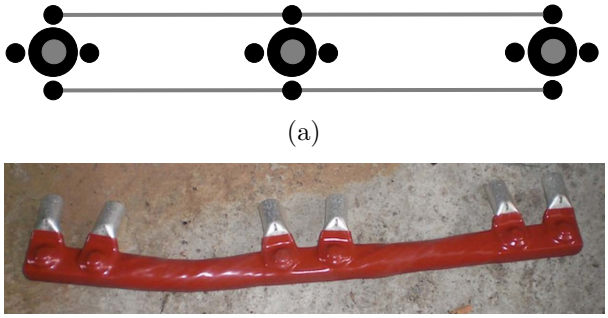

(a)

(b)

Figure 3.20: Layout of the ending connections (a) Realization of the ending connection (b).

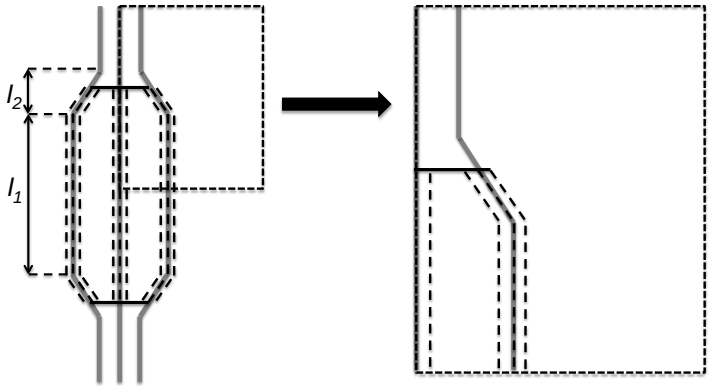

Figure 3.21: Junction zone: complete domain (left), 1/4 of the domain (right).

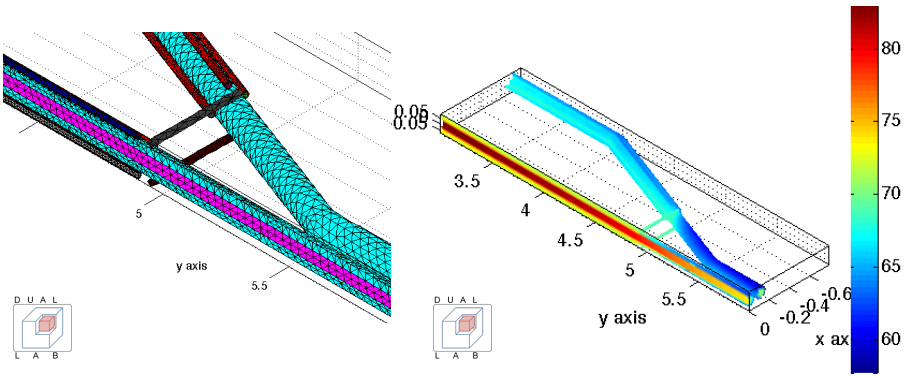

Figure 3.22: Junction zone: meshed domain (left), thermal field (right).

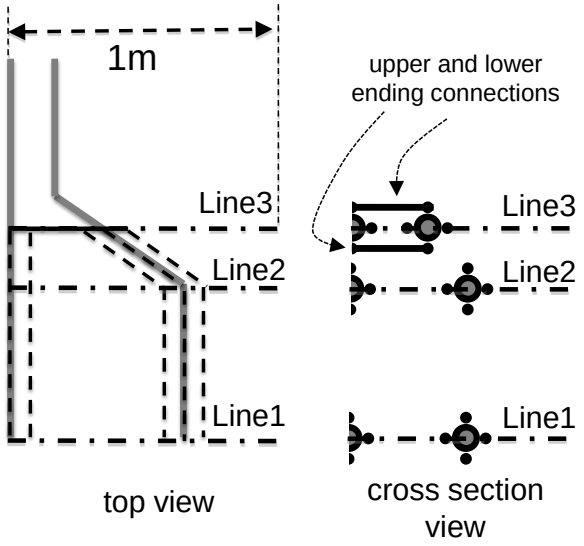

Figure 3.23: Reference lines for the temperature plot.

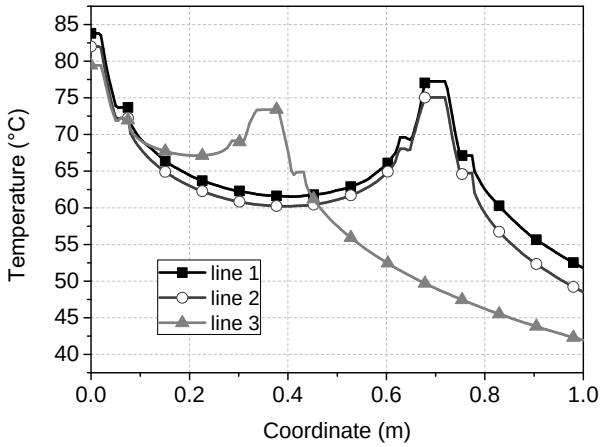

Figure 3.24: Temperature plot.

From the analysis of Fig. 3.24 it is possible to observe that the temperature for the central conductor is always decreasing going from the center of the junction zone to the trefoil arrangement (comparison of "line 1", "line 2" and "line 3" in the coordinate equal to zero). All the lines, after an initial decrease, present a second temperature peak that corresponds to the lateral power cables. The peak of the "line 3" (triangle symbol) is not located in the same place of the other two curves because the "line 3" intercepts the

lateral cables in a different position with respect to the previous reference lines. Peak temperature along "line 3" is lower than that along "line 1" because the volume heat generation due to shielding cables is limited to the part closed to the junction zone. Finally, the temperature of the lateral cable is (once again) decreasing going from the center of the junction zone to the trefoil arrangement, moreover, the temperature of the lateral cables is lower than the one of the central cable.
In conclusion, the vicinity of the shielding cables close to the ending connections does not imply an increase of temperature that leads to a thermal derating.

3.5.2 Thermal analysis of joints

Until now the joint zone has been analyzed without introducing the model of the joint: the joint zone had been considered only as an area where the distance between cables is higher. The joint is the point of the power line where two sections of cable are connected, so the geometry of this part is more complex. The cables junction is realized with different layers, but to perform the simulations it has been considered simply as an insulation layer with higher thickness. Because of the placement of the joints along the power line the whole domain can be reduced to an half of the domain, as represented in Fig. 3.25.

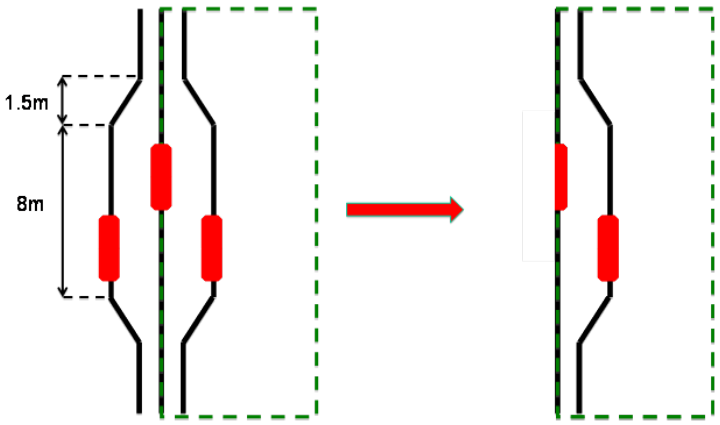

Figure 3.25: Joint zone: reduction of the domain.

At first the power line has been analyzed without the shielding system. In Fig. 3.26 it is shown the tridimensional model of the joint zone used in the simulations.
The simulation has been performed supplying the power line with a current value equal to the trefoil ampacity. In Fig. 3.27 the two inspection lines considered are shown: the red one is along the central cable, the blue one is along the external cable.
Without modelling the joints, in this area the temperature profile would be decreasing because of the greater distance between cables. The presence of the joints produces a local temperature increase along both the cables, but the temperature limit (90 °C) is

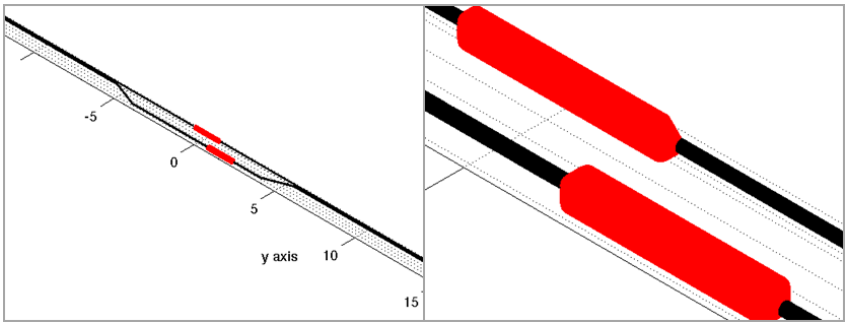

Figure 3.26: 3D model of the joint zone (left) and of the joint (right).

not reached in both the cases (Fig. 3.28). The central cable, that is the most stressed thermally, reaches in the joint zone the minimum temperature of 72 °C. Although the presence of joint produces an increase of temperature, because of the higher distance between the cables in this area of the power line, the joint does not cause a derating of the system. This result agrees with the conclusions of the analysis found in the Literature [35], [36].

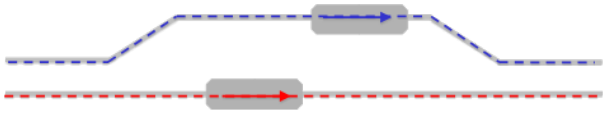

Figure 3.27: The inspection lines in the joint zone.

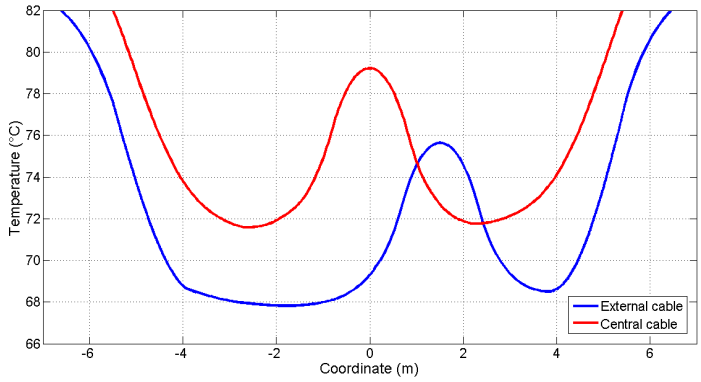

Figure 3.28: Temperature profile in the joint zone without HMCPL.

Then the previous model has been analyzed adding the HMCPL system with configuration 4 x 240 mm^2 (represented in green in Fig. 3.29). The simulation has been performed

supplying the power line with a current value equal to the ampacity obtained in the 2D analysis for this case.

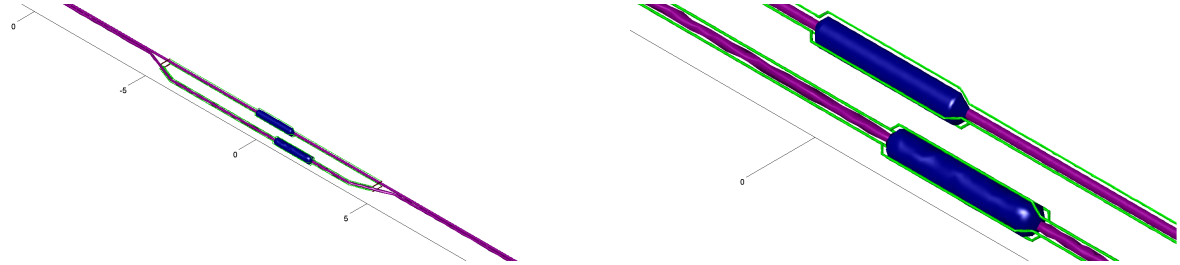

(a) (b)

Figure 3.29: 3D model of the joint zone (a) and of the joint (b) with HMCPL.

Considering the same inspection lines of the previous analysis (along the central and the external cable) the results obtained are shown in Fig. 3.30. As expected, for the presence of the shielding system, the cables temperature is higher respect to the previous case and the central cable is more stressed thermally than the external cable. In each cable the temperature local maximum is in correspondence to the respective joint. The temperature limit of 90 °C is reached only in the middle of the central cable joint. Therefore also the presence of HMCPL system does not cause a derating of the power line.
In conclusion, without or with the HMCPL system:

- the presence of the joint produces a local temperature increase along the power line;
- the local temperature increase is not restrictive for the performance of the system because in the joint zone the distance between cables is higher.

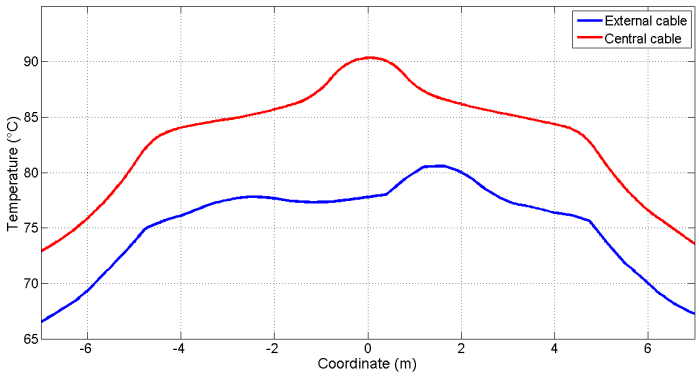

Figure 3.30: Temperature profile in the joint zone with HMCPL.

Finally a transient simulation has been performed for both the model of the joint zone (without and with HMCPL system). To study the transient behaviour in the joint zone four reference points have been chosen (Fig. 3.31):

- in the middle of the joint of the central cable (point A);
- in the middle of the joint of the external cable (point B);
- on the central cable in the joint zone (point C);
- on the central cable out the joint zone (point D).

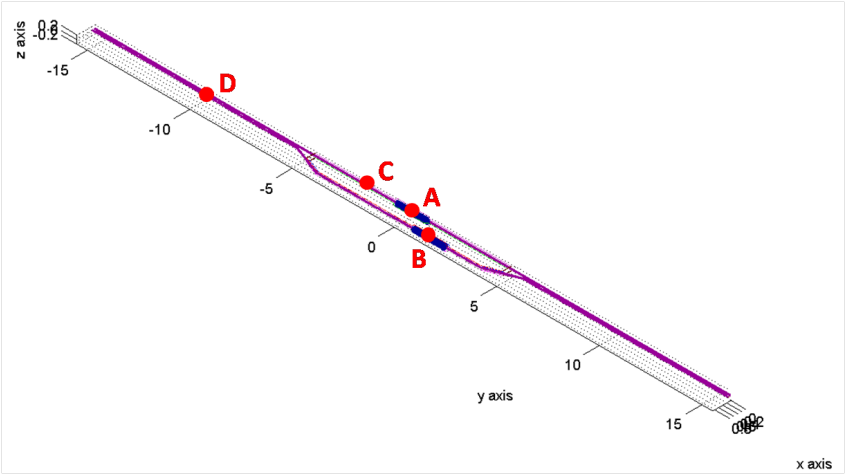

Figure 3.31: Reference points for transient analysis.

The results obtained by the transient analysis are summarized in Table 3.12. In absence of HMCPL point D is the most stressed thermally because in that part of the power line the cables are closer (trefoil configuration), so the temperature reached is higher. Point D has the shorter time constant respect to the other reference points: the time constants vary from 55 days (point D) to 66 days (point C). Adding the HMCPL point A becomes the hottest point, reaching the temperature limit of 90 °C, with a time constant of 61 days. The time constants vary from 61 days (points A and B) to 66 days (point C). In Fig. 3.32 and 3.33 the transient trends in the reference points are shown for both the models.

3.5.3 Fault configuration

In the previous paragraphs the normal operation of a power line with HMCPL was analyzed, without considering possible fault configurations. The most critical case for the power line is when the HMCPL shielding circuit is opened: in this case the magnetic core

Table 3.12: Time constant and steady-state temperature

Reference point	Model without HMCPL		Model with HMCPL	
	τ (days)	θ_{steady} (°C)	τ (days)	θ_{steady} (°C)
Point A	60	79	61	90
Point B	62	76	69	74
Point C	66	72	63	85
Point D	55	88	61	70

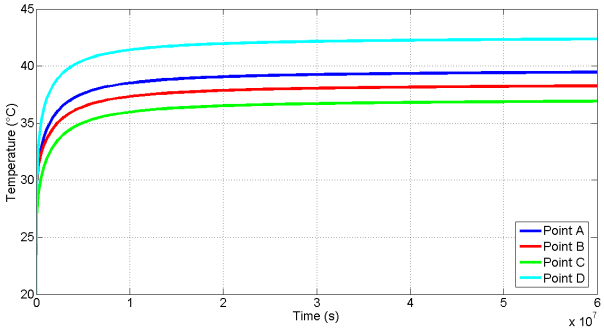

Figure 3.32: Transient in the reference points, model without HMCPL.

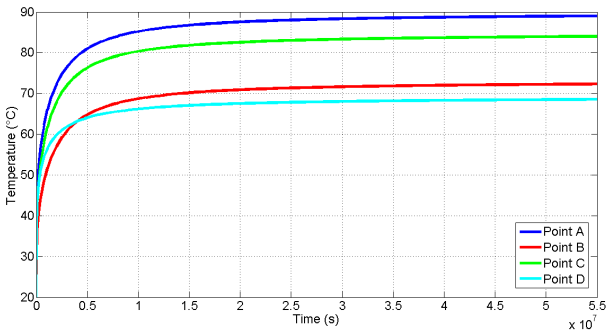

Figure 3.33: Transient in the reference points, model with HMCPL.

saturates because the source current becomes the magnetization current. The temperature of the magnetic core could increase because of the saturation of the magnetic core, damaging the source cable.
The opening of the shielding circuit is carefully avoided by means of protection against corrosion of the ending connections, but it is important to evaluate the temperature which the magnetic core reaches due to high saturation and its effect on the power cable.

First the model has been analyzed sperimentally, measuring the temperature on the magnetic core [37]. The measurements have been done under the following conditions:

- magnetic core supplied with primary current equal to 1000 A;
- secondary circuit not present;
- magnetic core thermally insulated from ground and primary power cable;
- 4 thermocouples for the magnetic core temperature;
- 1 thermocouple for environment temperature.

In Fig. 3.34 the experimental set-up is represented.

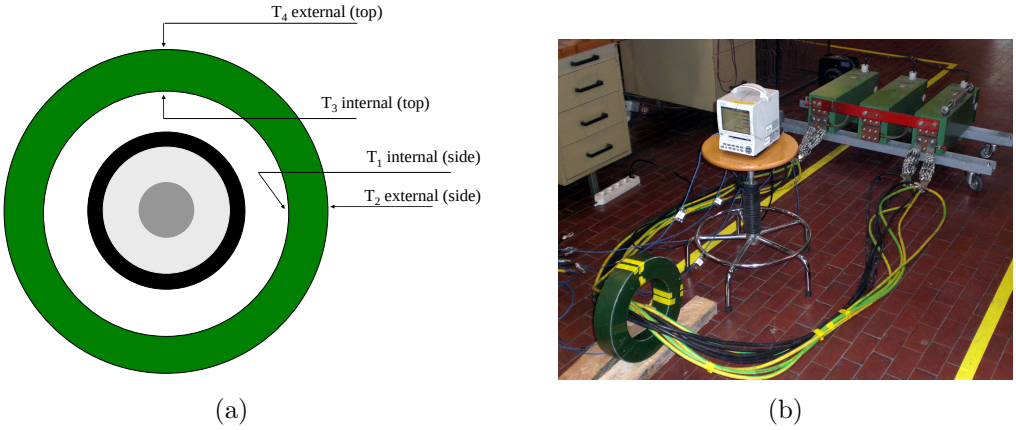

(a) (b)

Figure 3.34: Displacement of the thermocouples (a) Experimental set-up (b).

It is worth noting that the analyzed configuration is more critical than the practical one because, when the magnetic core is installed underground, the soil helps to keep the magnetic core temperature at lower level.
The temperature profile of the magnetic core during the fault configuration is shown in Fig. 3.35. The obtained curves have been fitted with the following equation:

$$\Delta\theta = \Delta\theta_0 + \Delta\theta_\infty \left(1 - e^{-t/\tau}\right) \tag{3.1}$$

where:

- $\Delta\theta = \theta - \theta_{ext}$ is the overtemperature on the magnetic core;
- $\Delta\theta_\infty$ is the overtemperature reached at the end of the thermal transient;
- τ is the time constant of the transient;

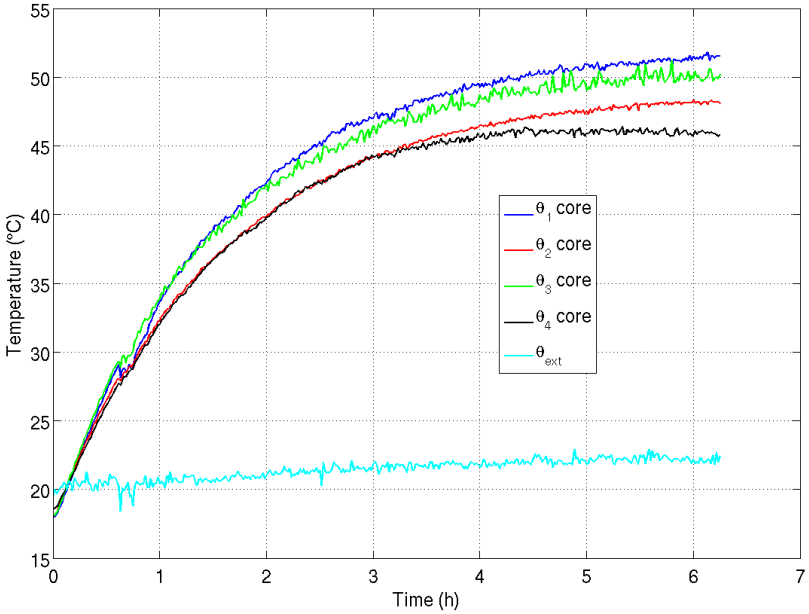

Figure 3.35: Magnetic core temperature during the fault configuration.

- $\Delta\theta_0$ is a variable which takes into account the overtemperature of the magnetic core respect to the environment at the beginning of the transient.

By fitting the curves represented in Fig. 3.35 it is possible to obtain the result of Fig. 3.36 where it is clearly represented the end of the transient. The maximum temperature (52 °C) is reached in the internal side of the magnetic core (θ_1): this temperature is far from the thermal limit of the insulation which is 90 °C. The time constant of the system (in air) is more or less 1.5 h. If the same configuration was installed underground the time constant would be higher because the thermal conductivity of soil is higher than the thermal conductivity of air.
Moreover, since the ground is able to exchange thermal energy with the magnetic core by means of thermal conduction, in order to prevent the heating of the power cable it is possible to install a thermal insulation between the power cable and the magnetic core so that, in fault configuration, the thermal dissipation of the Joule losses inside the core is imposed toward the external environment limiting the thermal flux toward the power cable.
Then the same model has been simulated by means of DualLab to know what is the effect of core losses on the cable temperature. The model analyzed is represented in Fig. 3.37, but considering the simmetries present in the model, only a quarter of the complete domain has been simulated, using the proper boundary conditions (Fig. 3.38).

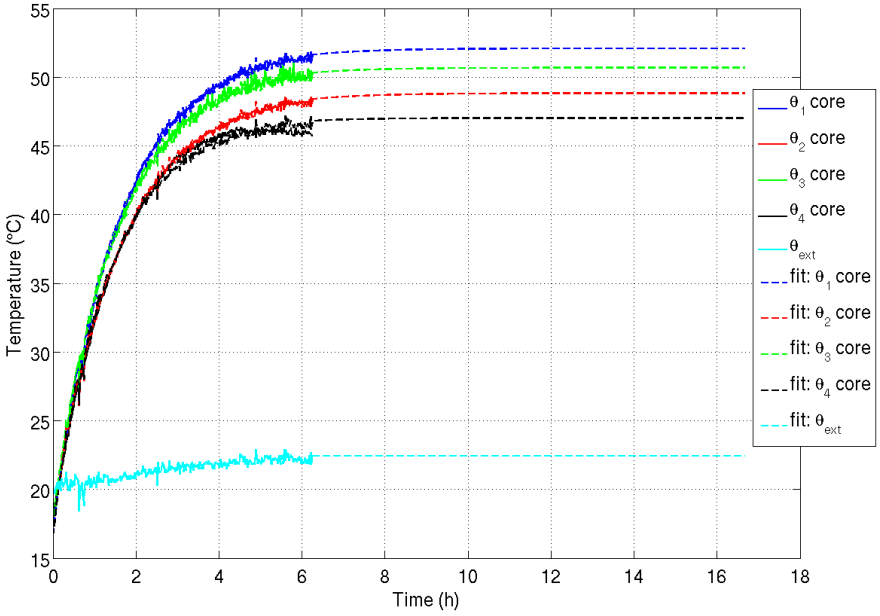

Figure 3.36: Magnetic core temperature during the fault configuration (fitted curve).

The simulated model is the real case, with the cable buried in the same conditions of the joint zone.

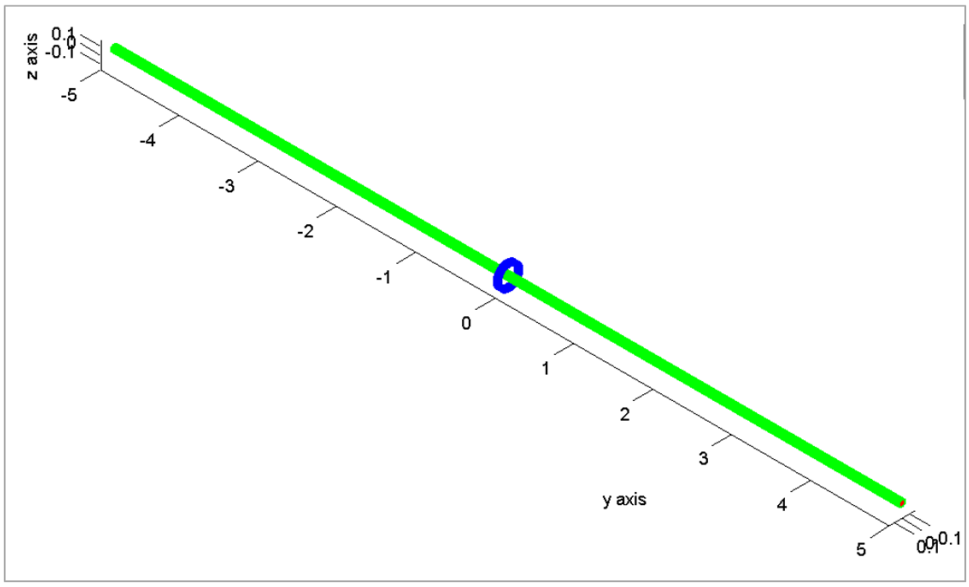

Figure 3.37: Fault configuration: complete domain.

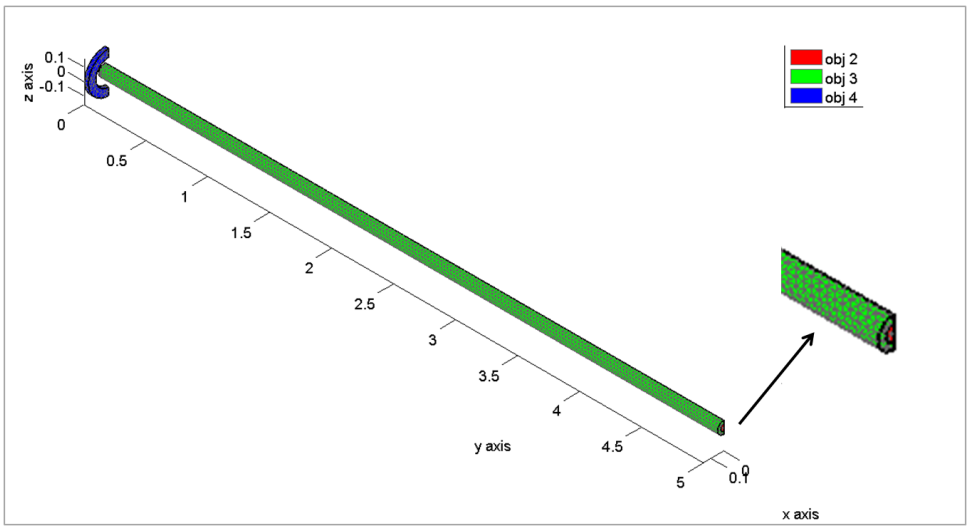

Figure 3.38: Fault configuration: reduced model.

In Fig. 3.39 the two reference lines considered are shown: line 1 along the axis of the cable (Fig. 3.39(a)) and line 2 along the axis of the magnetic core (Fig. 3.39(b)).
In this analysis the power line has been supplied with the current value that leads the cable to the temperature of almost 60 °C. This is the temperature reached by the central source cable of the joint zone where the magnetic core is installed (the model is the one considered in the previous paragraphs). Therefore considering only the Joule losses produced by the cable, the conductor has a temperature of almost 60 °C (blue line in Fig. 3.40 and 3.41).
If there were only the magnetic core losses, the temperature profile would be the one represented by the red line: the magnetic core reaches the temperature of 52 °C.
The green line represents the temperature profile for the complete model (Joule losses and magnetic core losses). The magnetic core contribute produces a temperature increase of about 10 °C in the cable in corrispondence of the magnetic core. Moving away from the core the effect of its losses decreases and the temperature difference decreases (the green line tends to the blue profile).
In case of fault of the HMCPL system circuit, the overtemperature reached by the magnetic core does not damage the source cable. In the case analyzed the source cable temperature increases of 10 °C, but the calculations done are conservative. To evaluate the losses inside the magnetic core it has been considered the case “in air” that is a case more critical. The magnetic core underground would reach a lower temperature and consequentely the cable overtemperature would be lower.

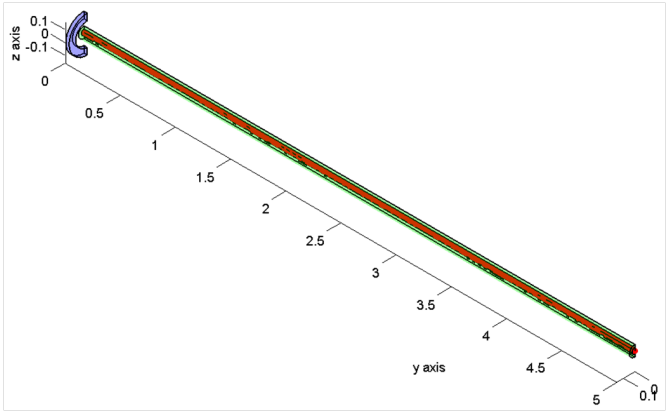

(a)

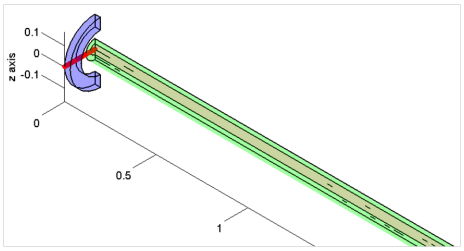

(b)

Figure 3.39: Reference line 1 (a) Reference line 2 (b).

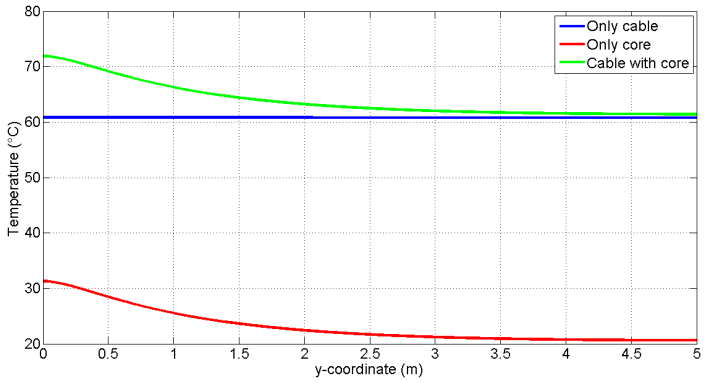

Figure 3.40: Temperature profile along the reference line 1.

3.6 Discussion of results

When the HMCPL is applied to a flat configuration the best magnetic performances are obtained by placing the shielding cables very close to the power lines, therefore a possible

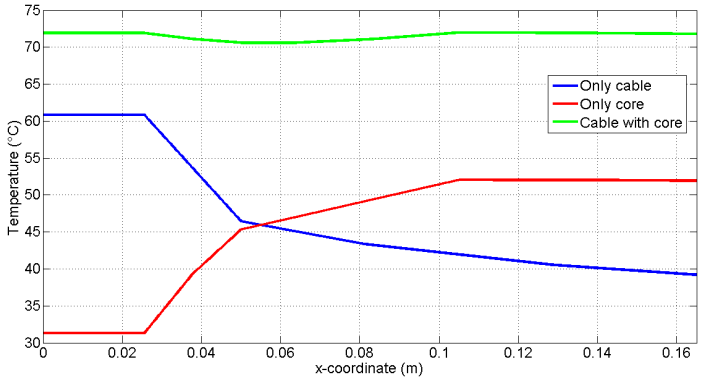

Figure 3.41: Temperature profile along the reference line 2.

derating of the system has to be taken into account. As a general conclusion, the insertion of the shielding cables reduces the ampacity of the power cables below the one of the trefoil configuration. It is worth noting that the overall effect of the HMCPL on the trefoil ampacity could be negligible when compared with other unavoidable bottlenecks along the power line path.
A further improvement of the analysis has been carried out by considering the thermal transient. Even if many configurations are subject to derating if analyzed in steady-state condition, the transient analysis shows how the thermal time constant of the system is higher than the variation of the load profile over 24 hours. This means that a huge amount of time is needed to achieve the actual steady-state temperature. This result is proven by simulating the most critical configuration based on a load profile with higher peaks than the computed ampacity and obtaining a temperature trend which is not as critical as foreseen by the steady-state simulation.
A 3D model of the junction zone with the HMCPL system has been taken into account for the investigation of the thermal behavior of the ending connections concluding that, even if the power cables are closer and the ending connection is another thermal source, the temperature is not critical if the system is well designed.
For a more detailed analysis, also the joint has been modelled. The presence of joint produces a peak temperature along the power line that is not restrictive for the operation of the power line.
Finally the fault configuration has been considered: when the HMCPL shielding circuit is open and the magnetic core saturates. The overtemperature reached by the magnetic core does not damage the source cable, whose temperature is far from the limit temperature (90 °C).

Chapter 4

Conclusions

The objective of the thesis was the analysis of the methodologies applicable in case of underground power cables, assessing when the existing standards are applicable and introducing other methods when the standards are not suitable.

Standards for cable ampacity calculation
The thermal analysis of cables aims at computing the temperature rise inside the cables due to the heat generated inside the conductor during the normal operation. Neher and McGrath in their paper introduced a method to calculate the temperature rise and the current-carrying capacity of cables and the Standards about this topic (the Standard IEEE 399-1997 and the Standard IEC 60287) found on this method.

Numerical methods application
The Standard IEC 60287 has been implemented by a MATLAB code. The ampacity for the test case (buried cables in flat configuration) has been calculated with both the MATLAB code and a commercial software, based on the Standard IEC 60287 too.
Fourteen different cases have been analyzed, considering the different methods of sheath bonding and two types of insulation (unfilled or filled XLPE). The results show that the type of sheath bonding has a big influence on the ampacity value. Then the same cases have been analyzed with a commercial code to test the correctness of the results obtained with the MATLAB code.

Thermal analysis of HMCPL
An application case has been considered: a power line arranged in flat configuration, shielded with passive loops (HMCPL technology). The use of HMCPL technology imposes the introduction of a new set of conductors and, consequently, new Joule losses in the system. Therefore a thermal analysis of the system is unavoidable in order to clarify whether the installation of a HMCPL leads to an ampacity derating of the power line or not.

To analyze this particular case both the MATLAB code and commercial software are not suitable because with them it is impossible to introduce external heat sources (the shield cables) and perform a 3D analysis (necessary to consider the effect of the ending connections). The Standard IEC 60287 does not consider these specific cases.
For these reasons all the simulations have been performed with DualLab, a MATLAB code that implements the cell method.
A steady-state analysis is not enough: even if many configurations are subject to derating if analyzed in steady-state conditions, the transient analysis shows how the thermal time constant of the system is higher than the variation of the load profile over 24 h.
Finally, a 3D model of the junction zone with the HMCPL system has been taken into account for the investigation of the thermal behavior of the ending connections concluding that, even if the power cables are closer and the ending connection is another thermal source, the temperature is not critical if the system is well designed.
Even in case of fault of the HMCPL system circuit the power line cables are not damaged. The magnetic core losses are an additional heat contribute. This losses contribute produces a temperature increase in the source cables, but the temperature reached by the source cables is far from the temperature limit.

Bibliography

[1] J. Neher and H. McGrath, "The calculations of the temperature rise and load capability of cable systems," *AIEE Transactions on Power Applications Systems*, vol. 76, pp. 752–772, Oct. 1957.

[2] P. Pollak, "Neher-McGrath calculations for insulated power cables," *IEEE Transactions on Industry Application*, vol. IA-21, September/October 1985.

[3] "IEEE Std 399-1997, IEEE Recommended Practice for Industrial and Commercial Power Systems Analysis."

[4] H. M. Knutson and B. B. Miles, "Cable derating parameters and their effects," *IEEE paper*, no. PCIC-77-5, 1977.

[5] "NFPA 70-1996, National Electrical Code (NEC)."

[6] "IEEE Std 835-1994, Standard Power Cable Ampacity Tables."

[7] EEI Publication, *Underground Systems Reference Book*. No. 55-16, Edison Electric Institute, New York City, NY, 1957.

[8] "IEC Std 60287 Electric cables - Calculation of the current rating, 2006."

[9] G. Bazzi, "Riduzione delle perdite nelle guaine metalliche dei cavi unipolari mediante trasposizione incrociata," *AEI - L'ELETTROTECNICA*, vol. 58, pp. 216–227, 1971.

[10] F. Freschi, L. Giaccone, and M. Repetto, "Educational value of the algebraic numerical methods in electromagnetism," *COMPEL*, vol. 27, no. 6, pp. 1343–1357, 2008.

[11] D. Villaci and A. Vaccaro, "Transient tolerance analysis of power cables thermal dynamic by interval mathematic," *Electric Power System Research*, vol. 77, pp. 308–314, 2007.

[12] M. S. Al-Saud, M. A. El-Kady, and R. D. Findlay, "A new approach to underground cable performance assessment," *Electric Power Systems Research*, vol. 78, pp. 907–918, 2008.

[13] "Review of the scientific evidence for limiting exposure to electromagnetic fields (0-300 ghz)," Tech. Rep. Vol. 15 N.3, National Radiological Protection Board, 2004.

[14] "Mitigation techniques of power frequency magnetic fields originated from electric power systems," Tech. Rep. Worging group C4.204, International Council on Large Electric Systems (CIGRE'), 2009, ISBN: 978-2-85873-060-5.

[15] B. Shperling, L. Menemenlis-Hopkins, B. Fardanesh, B. Clairmont, and D. Child, "Reduction of magnetic fields from transmission lines using passive loops," in *Cigré 1996 - Paper 36-103*, 1996.

[16] A. Canova and L. Giaccone, "Optimal design of high magnetic coupling passive loop for power lines field mitigation," *COMPEL*, vol. 28, pp. 1294–1308, 2009.

[17] A. Canova and L. Giaccone, "Magnetic field mitigation of power cable by high magnetic coupling passive loop," in *The 20th International Conference and Exhibition on Electricity Distribution, CIRED 2009.*, Prague, Czech Republic, 8-11 June 2009.

[18] A. Canova and L. Giaccone, "Sistema di schermatura passiva di tipo magliato e conduttivo ad elevato accoppiamento magnetico." Patent n. TO2008A000176, 2008.

[19] A. Canova and L. Giaccone, "Passive shielding system of a meshed and conductive type with high magnetic coupling passive loop." PCT/IB2009/000445, 2009.

[20] A. Canova and L. Giaccone, "A novel technology for magnetic-field mitigation: High magnetic coupling passive loop," *IEEE Transactions on Power Delivery*, vol. Vol. 26, pp. 1625 – 1633, July 2011.

[21] A. Canova, F. Freschi, L. Giaccone, and A. Guerrisi, "The high magnetic loop passive loop: A steady-state and transient analysis of the thermal behavior," *Applied Thermal Engineering*, vol. 37, pp. 154–164, 2012.

[22] T. L. Jones, "The calculation of cable parameters using combined thermal and electrical circuit models," *IEEE Transactions on Power Delivery*, vol. 4, no. 3, pp. 1529–1540, 1989.

[23] G. Mazzanti, "Analysis of the combined effects of load cycling, thermal transients, and electrothermal stress on life expectancy of high-voltage ac cables," *IEEE Transactions on Power Delivery*, vol. 22, no. 4, pp. 2000–2009, 2007.

[24] M. Hanna, A. Chikhani, and M. Salama, "Thermal analysis of power cables in multi-layered soil. part 1. theoretical model," *IEEE Transactions on Power Delivery*, vol. 8, no. 3, pp. 761–771, 1993.

[25] C. Hwang, "Calculation of thermal fields of underground cable systems with consideration of structural steels constructed in a duct bank," *IEE Proceedings-Generation, Transmission and Distribution*, vol. 144, no. 6, pp. 541–545, 1997.

[26] J. Nahman and M. Tanaskovic, "Determination of the current carrying capacity of cables using the finite element method," *Electric Power Systems Research*, vol. 61, pp. 109–117, 2002.

[27] C. C. Hwang and Y. Jiang, "Extensions to the finite element method for thermal analysis of underground cable systems," *Electric Power Systems Research*, vol. 64, pp. 159–164, 2003.

[28] R. de Lieto Vollaro, L. Fontana, and A. Vallati, "Thermal analysis of underground electrical power cables buried in non-homogeneous soils," *Applied Thermal Engineering*, vol. 31, pp. 772–778, 2011.

[29] C. C. Hwang, J. J. Chang, and Y. H. Jiang, "Analysis of electromagnetic and thermal fields for a bus duct system," *Electric Power Systems Research*, vol. 45, pp. 39–45, 1998.

[30] N. Kovac, I. Sarajcev, and D. Poliak, "Nonlinear-coupled electric-thermal modeling of underground cable systems," *IEEE Transactions on Power Delivery*, vol. Vol. 21, pp. 4–14, 2006.

[31] "Guidelines for limiting exposure to time varying electric, magnetic and electromagnetic fields (up to 300 ghz)." International Commission on Non-Ionizing Radiation Protection (ICNIRP), 1998.

[32] M. Hanna, A. Chikhani, and M. Salama, "Thermal analysis of power cables in multi-layered soil. part 2. practical considerations," *IEEE Transactions on Power Delivery*, vol. 8, no. 3, pp. 772–778, 1993.

[33] J. Desmet, D. Putman, G. Vanalme, R. Belmans, and D. Vandommelen, "Thermal analysis of parallel underground energy cables," in *Proc. of the 18th International Conference on Electricity Distribution*, Turin, 6-9 June 2005.

[34] A. Canova and L. Giaccone, "Application of high magnetic passive loop to the magnetic mitigation of hv junction zone," in *2nd International Conference on EMF ELF - paper 54*, (Paris), Mar 24^{th}-25^{th}, 2011.

[35] J. A. Pilgrim, D. J. Swaffield, P. L. Lewin, S. T. Larsen, and D. Payne, "Assessment of the impact of joint bays on the ampacity of high-voltage cable circuits," *IEEE Transactions On Power Delivery*, vol. 24, 2009.

[36] CIGRE' Study Committee B1, "Thermal ratings of hv cable accessories," tech. rep., 2012.

[37] L. Giaccone, *Magnetic field mitigation of underground power lines.* PhD thesis, Politecnico di Torino, 2010.